© 2018. Published by The Company of Biologists Ltd | Journal of Cell Science (2018) 131, jcs221994. doi:10.1242/jcs.221994

RESEARCH ARTICLE

Constitutive $P2Y_2$ receptor activity regulates basal lipolysis in human adipocytes

Seema B. Ali[1], Jeremy J. O. Turner[2] and Samuel J. Fountain[1,*]

ABSTRACT

White adipocytes are key regulators of metabolic homeostasis, which release stored energy as free fatty acids via lipolysis. Adipocytes possess both basal and stimulated lipolytic capacity, but limited information exists regarding the molecular mechanisms that regulate basal lipolysis. Here, we describe a mechanism whereby autocrine purinergic signalling and constitutive $P2Y_2$ receptor activation suppresses basal lipolysis in primary human *in vitro*-differentiated adipocytes. We found that human adipocytes possess cytoplasmic Ca^{2+} tone due to ATP secretion and constitutive $P2Y_2$ receptor activation. Pharmacological antagonism or knockdown of $P2Y_2$ receptors increases intracellular cAMP levels and enhances basal lipolysis. $P2Y_2$ receptor antagonism works synergistically with phosphodiesterase inhibitors in elevating basal lipolysis, but is dependent upon adenylate cyclase activity. Mechanistically, we suggest that the increased Ca^{2+} tone exerts an anti-lipolytic effect by suppression of Ca^{2+}-sensitive adenylate cyclase isoforms. We also observed that acute enhancement of basal lipolysis following $P2Y_2$ receptor antagonism alters the profile of secreted adipokines leading to longer-term adaptive decreases in basal lipolysis. Our findings demonstrate that basal lipolysis and adipokine secretion are controlled by autocrine purinergic signalling in human adipocytes.

KEY WORDS: Adipose tissue, Purinergic receptor, Calcium signalling, Human

INTRODUCTION

White adipose tissue (WAT) is the primary site of long-term energy storage within mammals. WAT comprises a diverse range of cells, of which the predominant cell type is white adipocytes. White adipocytes play a pivotal role in the endocrine function of WAT, via the production and release of adipokines to regulate systemic metabolism (Halberg et al., 2008). However, their primary function is to facilitate long-term storage of excess nutrients within large lipid droplets. These lipid droplets give white adipocytes their distinctive unilocular morphology. Adipocytes are highly dynamic cells, which store excess energy in the form of triglycerides in the fed state via lipogenesis and release energy in the form of free fatty acids during fasting via lipolysis (Rutkowski et al., 2015). The metabolic activity of white adipocytes is regulated tightly by hormones and the autonomic nervous system to achieve whole-body metabolic homeostasis. As such, loss of adipocyte control is associated with cardiovascular risk and obesity (Nielsen et al., 2014; Rosen and Spiegelman, 2006). Adipocytes possess both a basal and stimulated lipolytic capacity. The most well-characterised stimulated lipolytic pathway is mediated by sympathetic nerve stimulation of WAT via β-adrenoreceptors. Upon activation of β-adrenoreceptors, G_s-mediated stimulation of adenylate cyclase is initiated, which causes an elevation in cytoplasmic cyclic adenosine monophosphate (cAMP). Subsequently, this activates protein kinase A (PKA), which, in turn, phosphorylates hormone-sensitive lipase (HSL; also known as LIPE) and perilipins on the surface of the lipid droplet to allow translocation of HSL to the lipid droplet (Miyoshi et al., 2006), where HSL, in combination with adipose triglyceride lipase (ATGL) and monoglyceride lipase (MGL; also known as MGLL), catalyses the hydrolysis of triglycerides to free fatty acids and glycerol molecules. The free fatty acids can then be released into the bloodstream, where they are able to travel to distant organs and be utilised as a cellular energy source (Ahmadian et al., 2010). Despite the importance of basal lipolysis in regulating adipose tissue volume and the level of circulating free fatty acids (Heckmann et al., 2014; Miyoshi et al., 2008; Rydén and Arner, 2017), the molecular mechanisms regulating basal lipolysis are less well defined than the stimulated lipolytic pathways.

The concentration of free cytoplasmic Ca^{2+} and the rhythmicity of Ca^{2+} oscillations within the cytoplasm are critical regulators of many important processes within mammalian cells, including gene expression, cytoskeletal rearrangement, secretion and metabolism (Clapham, 2007). In adipocytes, intracellular Ca^{2+} is known to be a key regulator of adipocyte differentiation (Shi et al., 2000) and metabolism (Arruda and Hotamisligil, 2015), but cell surface receptors that evoke intracellular Ca^{2+} responses and how they are linked to metabolic control of human adipocytes are poorly defined.

Adipocytes in WAT are innervated by the sympathetic branch of the autonomic nervous system (Bartness et al., 2014). Increased sympathetic tone drives lipolysis through the action of noradrenaline on β-adrenergic receptors expressed at the adipocyte cell surface (Ahmadian et al., 2010). Consequently, local denervation of white adipose depots in pre-clinical models leads to fat pad expansion (Bowers et al., 2004). Sympathetic neurons release adenosine triphosphate (ATP) as a co-transmitter with noradrenaline during innervation of a range of tissues (Kennedy, 2015). In addition, ATP is also released physiologically by cells during inflammation and injury, when it acts as a danger-associated molecular pattern (Gorini et al., 2013). We and others have also documented constitutive release of ATP by differing mammalian cell types (Corriden and Insel, 2010; Sivaramakrishnan et al., 2012), which produces a resting steady concentration of ATP close to the cell surface and tonic activation of some purinergic receptor subtypes. Extracellular ATP can evoke changes in cytoplasmic Ca^{2+} via activation of P2X and P2Y cell surface purinergic receptors. P2X receptors ($P2X_{1–7}$) are non-selective ligand-gated ion channels activated by extracellular ATP that directly permeate to Ca^{2+} (North, 2002). P2Y receptors

[1]Biomedical Research Centre, School of Biological Sciences, University of East Anglia, NR4 7TJ Norwich, UK. [2]Norfolk and Norwich University Hospital, Colney Lane, NR4 7TJ Norwich, UK.

*Author for correspondence (s.j.fountain@uea.ac.uk)

S.J.F., 0000-0002-6028-0548

Received 26 June 2018; Accepted 5 October 2018

Journal of Cell Science (2018) 131, jcs221994. doi:10.1242/jcs.221994

($P2Y_{1,2,4,6,11–14}$) are G protein-coupled receptors that are activated by ATP, adenosine diphosphate (ADP), uridine-5′-triphosphate (UTP), uridine diphosphate (UDP) and UDP-sugars in a subtype-specific manner (von Kügelgen and Hoffmann, 2016). $P2Y_{1,2,4,6,11}$ are G_q-coupled receptors, so upon activation they elevate cytoplasmic Ca^{2+} through IP3-mediated release of Ca^{2+} stored in the endoplasmic reticulum. $P2Y_{13}$ and $P2Y_{14}$ receptors are G_i coupled and evoke pertussis toxin-sensitive intracellular Ca^{2+} responses. $P2Y_{12}$ receptors are also G_i coupled, but do not evoke intracellular Ca^{2+} responses; instead, they positively regulate intracellular Ca^{2+} responses evoked by other P2Y receptors (Micklewright et al., 2018). The repertoire and function of cell surface purinergic receptors expressed by human adipocytes is currently unclear. Here, we sought to determine which purinergic receptors are expressed by primary human *in vitro*-differentiated adipocytes and investigate their potential in regulating basal lipolysis.

RESULTS

ATP-, ADP- and UTP-evoked intracellular Ca^{2+} responses in human adipocytes

A representative image of human adipose-derived mesenchymal stromal cells differentiated to mature adipocytes following the habituation protocol is shown in Fig. 1A. Application of exogenous ATP, ADP and UTP evoked intracellular Ca^{2+} responses in adipocytes (Fig. 1B) with a rank order of potency of ADP [half-maximal effective concentration (EC_{50}) 239±48.1 nM; *N*=6]>ATP (EC_{50} 1.84±1.42 µM; *N*=6)>UTP (EC_{50} 13.0±4.6 µM; *N*=6) (Fig. 1C). The magnitude of the responses at maximal agonist concentrations also had the rank order of ADP>ATP>UTP (Fig. 1D). *In vitro*-differentiated adipocytes were unresponsive to UDP (<30 µM) and UDP-glucose (<100 µM) (*N*=6) (data not shown).

ATP responses were metabotropic in nature as responses persisted in the absence of extracellular Ca^{2+} (Fig. 1E,F), but were abolished following phospholipase C inhibition with U73122 (Fig. 1G,H). However, the responses to ATP decreased in the absence of extracellular Ca^{2+}, which suggests that extracellular Ca^{2+} is important for the magnitude of the response. We next used selective receptor antagonists to probe the molecular basis of nucleotide-evoked Ca^{2+} responses in human adipocytes. ATP-evoked responses were attenuated following selective antagonism of $P2Y_1$, $P2Y_2$ and $P2Y_{12}$ receptors with MRS2500 [half-maximal inhibitory concentration (IC_{50}) 415±160 nM; *N*=6], AR-C118925XX (IC_{50} 683±116 nM; *N*=6; Rafehi et al., 2017) and PSB-0739 (IC_{50}>10 µM; *N*=6), respectively (Fig. 2A–D; Table S1). The responses could be inhibited further by combining $P2Y_1$, $P2Y_2$ and $P2Y_{12}$ selective antagonists (Fig. 2E), suggesting that, in addition to the ATP/UTP-activated $P2Y_2$ receptor, ADP-activated receptors $P2Y_1$ and $P2Y_{12}$ actively contribute to the ATP response.

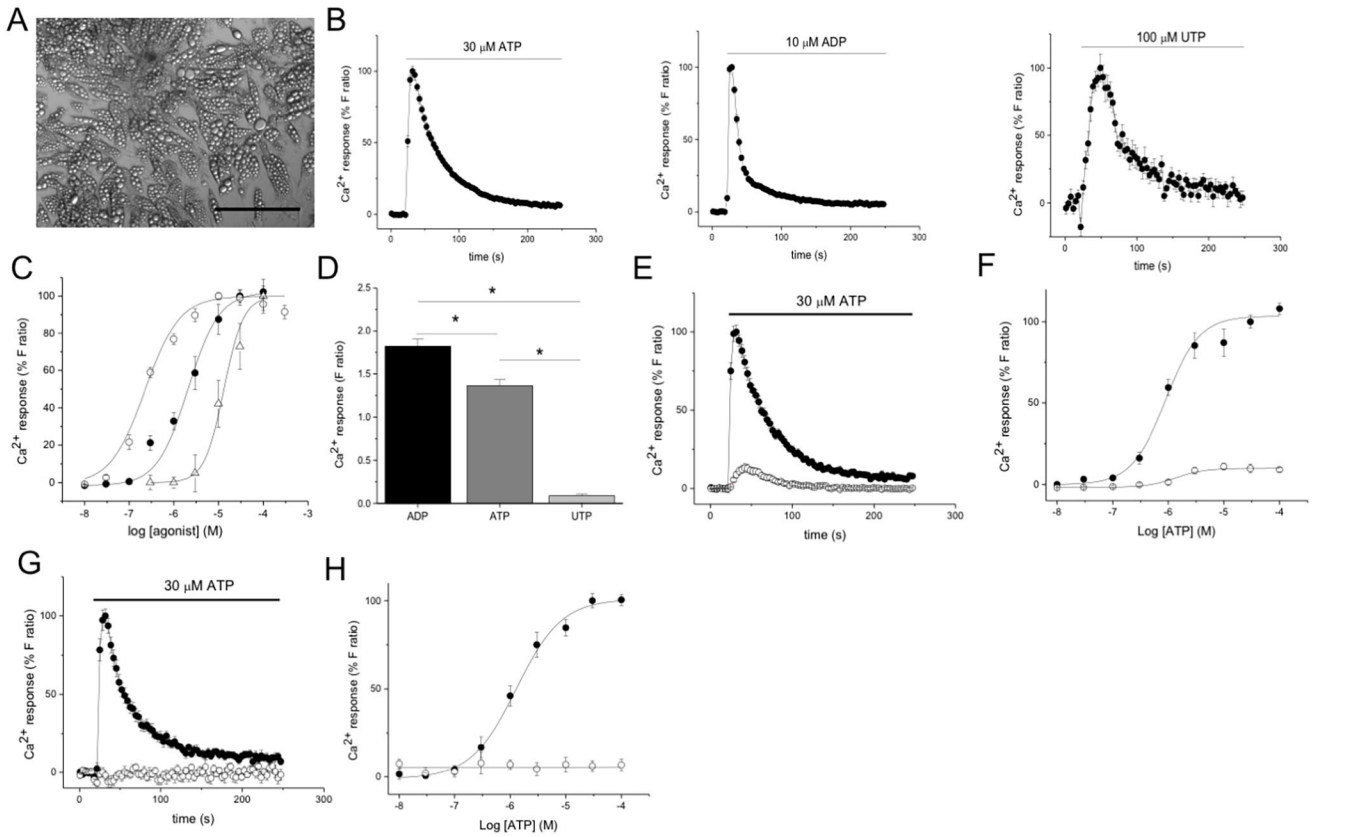

Fig. 1. Extracellular ATP-, ADP- and UTP-elicited intracellular Ca^{2+} responses in human adipocytes. (A) Representative image of human adipocytes in culture. Scale bar: 100 µm. (B) Time-resolved intracellular Ca^{2+} responses for maximal concentrations of ATP, ADP and UTP (*N*=6). Traces are normalised to peak response. (C) Concentration-response relationship for Ca^{2+} responses evoked by ATP (closed circles), ADP (open circles) and UTP (open triangles) (*N*=6). (D) Significant differences in Ca^{2+} response maxima evoked by nucleotides at maximal concentrations (ATP, 30 µM; ADP, 10 µM; UTP, 100 µM) (*N*=6; *P<0.05). (E) Time-resolved intracellular Ca^{2+} response evoked by ATP in the presence (closed circles) and absence (open circles) of extracellular Ca^{2+} (*N*=6). (F) ATP concentration response curve in the presence (closed circles) and absence (open circles) of extracellular Ca^{2+} (*N*=6). (G) Effect of phospholipase C inhibition on intracellular Ca^{2+} responses evoked by ATP. Ca^{2+} signal evoked by ATP in the presence (open circles) and absence (closed circles) of 10 µM U73122 (*N*=6). (H) Concentration-response curve for ATP in the presence (open circles) and absence (closed circles) of 10 µM U73122 (*N*=6). The F_{ratio} represents the emission ratio of Fura-2AM throughout. *N* represents the number of donors (biological repeats).

Journal of Cell Science (2018) 131, jcs221994. doi:10.1242/jcs.221994

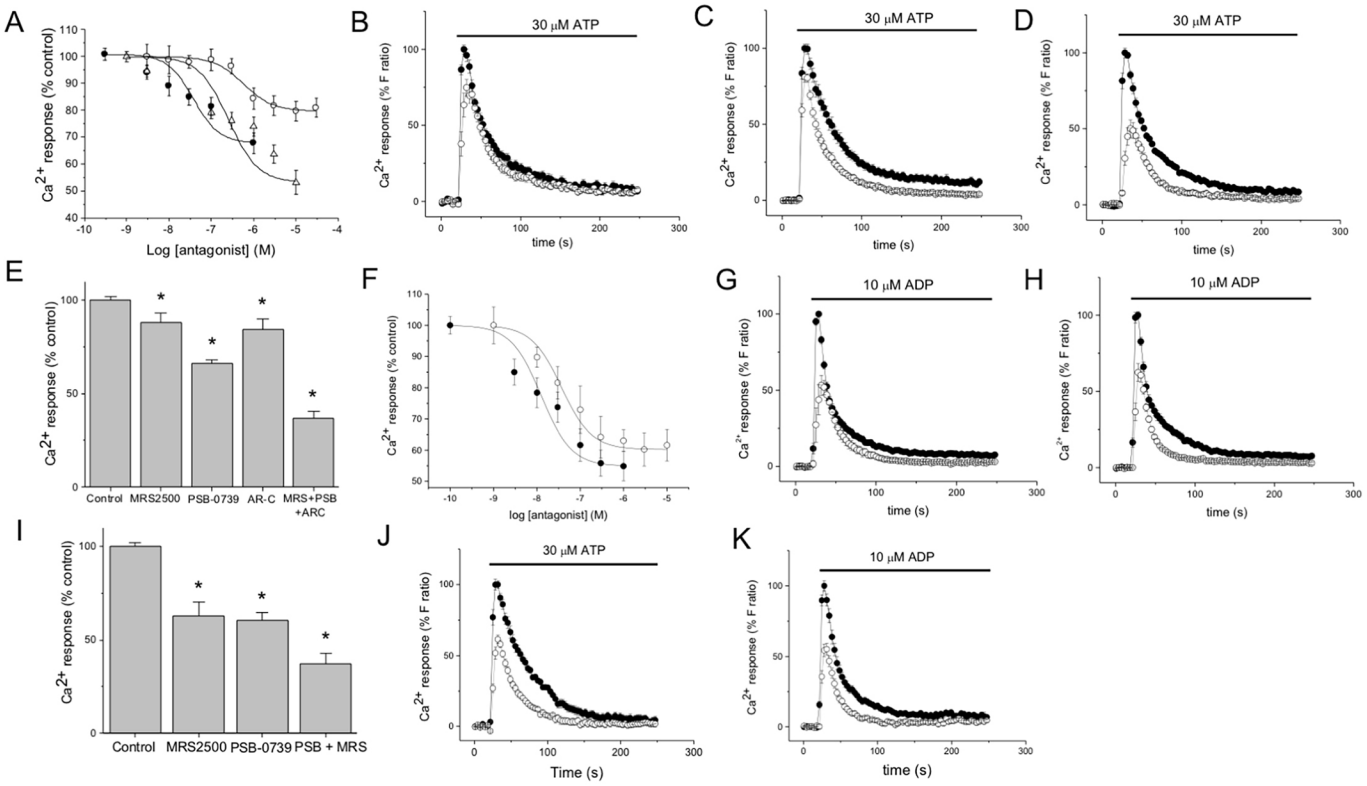

Fig. 2. $P2Y_1$, $P2Y_2$ and $P2Y_{12}$ receptor activation mediates ATP-evoked Ca^{2+} signalling, and $P2Y_1$ and $P2Y_{12}$ receptor activation mediates ADP-evoked Ca^{2+} signalling, in human adipocytes. (A) Effect of P2Y subtype-selective antagonists on Ca^{2+} responses evoked by 30 µM ATP. Concentration-inhibition curve for MRS2500 ($P2Y_1$; closed circles), AR-C118925XX ($P2Y_2$; open circles) and PSB0739 ($P2Y_{12}$; open triangles) (*N*=6). Responses are normalised to the agonist response in the presence of vehicle control only. (B–D) Time-resolved Ca^{2+} response evoked by ATP in the presence (open circles) and absence (closed circles) of 1 µM MRS2500 (B), 10 µM AR-C118925XX (C) or 10 µM PSB-0739 (D) (*N*=6). Traces are normalised to peak agonist response in the presence of vehicle control only. (E) Effects of individual antagonists (MRS2500, 1 µM; AR-C118925XX, 10 µM; PSB-0739, 3 µM), or in combination, on the magnitude of Ca^{2+} response evoked by 30 µM ATP (*N*=6; **P*<0.05 versus vehicle control). (F) Effect of $P2Y_1$ and $P2Y_{12}$ receptor antagonist subtype-selective inhibitors on Ca^{2+} responses evoked by 10 µM ADP. Concentration-inhibition curve for MRS2500 ($P2Y_1$; closed circles) and PSB-0739 ($P2Y_{12}$; open circles) (*N*=6). (G,H) Time-resolved Ca^{2+} response evoked by ADP in the presence (open circles) and absence (closed circles) of 1 µM MRS2500 (G), 3 µM PSB-0739 (H) (*N*=6). (I) Effects of individual antagonists (MRS2500, 1 µM; PSB-0739, 3 µM), or in combination, on the magnitude of Ca^{2+} response evoked by 10 µM ADP (*N*=6; **P*<0.05 versus vehicle control). (J,K) Effect of 100 ng/ml pertussis on Ca^{2+} responses evoked by ATP (J) or ADP (K). Traces shown are for vehicle control (closed circles) or with pertussis toxin (open circles). The F_{ratio} represents the emission ratio of Fura-2AM throughout. *N* represents the number of donors (biological repeats).

This is likely to be due to ectonucleotidase breakdown of extracellular ATP to ADP (Yegutkin, 2008). Contribution of $P2Y_1$ receptors to the ATP/ADP response is expected due to its G_q coupling; however, the contribution of the G_i-coupled $P2Y_{12}$ receptor is less expected, although not unprecedented, as it has been shown in other cell types (Micklewright et al., 2018). In addition, $P2Y_1$ (MRS2500; IC_{50} 77.1±37.5 nM; *N*=6; Kim et al., 2003) or $P2Y_{12}$ (PSB-0739; IC_{50} 64.0±56.5 nM; *N*=6; Hoffman et al., 2009) receptor antagonism attenuated ADP-evoked Ca^{2+} signalling in adipocytes (Fig. 2F,H), with further attenuation observed when the antagonists were combined (Fig. 2I). A role for $P2Y_{12}$ and G_i coupling was further substantiated as pertussis toxin, an inhibitor of G_i signalling (Katada et al., 1983), inhibited both the ATP- and ADP-evoked intracellular Ca^{2+} responses in human adipocytes (Fig. 2J,K).

P2Y receptor expression in human adipocytes and human adipose tissue

Analysis by quantitative RT-PCR revealed a diverse expression profile of purinergic receptors in human adipocytes, including $P2X_{4–7}$, $P2Y_1$, $P2Y_2$, $P2Y_4$, $P2Y_6$, $P2Y_{11}$, $P2Y_{12}$ and $P2Y_{13}$, whereas $P2X_1$, $P2X_2$, $P2X_3$ and $P2Y_{14}$ are not expressed (Fig. 3A). The same receptor subtypes were detected by immunocytochemistry in adipocytes *in vitro* (Fig. 3B). The expression of $P2Y_1$, $P2Y_2$ and $P2Y_{12}$ is supported by the functional pharmacology presented (Fig. 2). However, despite detection at the mRNA and protein level, the use of selective antagonists for $P2X_4$ (≤30 µM PSB12062; Hernadez-Olmos et al., 2012), $P2X_7$ (≤10 µM A438079; Nelson et al., 2006), $P2Y_6$ (≤10 µM MRS2578; Mameddova et al., 2004), $P2Y_{11}$ (≤10 µM NF340; Meis et al., 2010) and $P2Y_{13}$ (≤3 µM MRS2211; Kim et al., 2005) had no effect on ATP- and/or ADP-evoked intracellular Ca^{2+} responses in adipocytes (Table S1), suggesting that these subtypes are not involved under the conditions tested. $P2Y_1$, $P2Y_2$ and $P2Y_{12}$ expression was also confirmed in adipocytes in sections of human subcutaneous adipose tissue (Fig. 3C).

Constitutive $P2Y_2$ receptor activity produces intracellular Ca^{2+} tone

Extracellular ATP is known to act both as a paracrine and autocrine signal, and we and others have previously observed some mammalian cells to have a halo of extracellular ATP due to constitutive release (Corriden and Insel, 2010; Sivaramakrishnan et al., 2012). To this end, we sought to investigate the ability of human adipocytes to secrete ATP and the impact this has on homeostasis. Bulk-phase luminometry measurements of ATP

Journal of Cell Science (2018) 131, jcs221994. doi:10.1242/jcs.221994

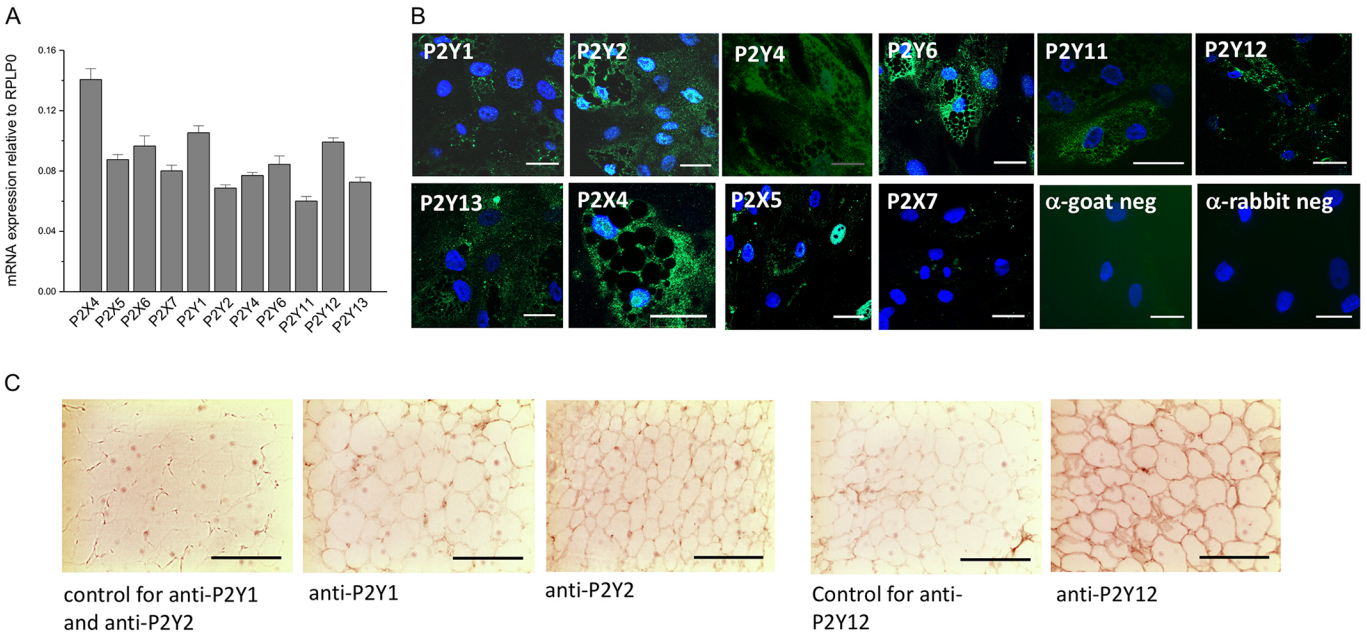

Fig. 3. Expression of purinergic receptors in human adipocytes and adipose tissue. (A) Quantitative RT-PCR analysis of P2Y and P2X receptor subtypes expressed by adipocytes (*N*=6 donors). Expression is given relative to the housekeeper gene, *RPLP0*. (B) Immunocytochemical staining of purinergic receptor subtypes in human adipocytes. Rabbit polyclonal primary antibodies against $P2X_4$, $P2X_7$, $P2Y_1$, $P2Y_2$, $P2Y_4$, $P2Y_6$, $P2Y_{11}$, $P2Y_{13}$ receptors, and goat polyclonal primary antibodies against $P2X_5$ and $P2Y_{12}$ receptors, are used. The green channel shows fluorescence arising from secondary anti-rabbit or anti-goat Alexa Fluor 488-conjugated antibodies (α-goat neg or α-rabbit neg) non-specific binding negative controls for secondary antibodies. The blue channel shows nuclei counterstained with DAPI. Scale bars: 30 µm. Images are representative of at least ten fields of view for three donors. (C) Anti-$P2Y_1$, anti-$P2Y_2$ and anti-$P2Y_{12}$ immunoreactivity in 6 µm sections of human abdominal subcutaneous WAT. Immunoreactivity was visualised using a horseradish peroxidase (HRP)-conjugated secondary antibody. Non-specific secondary binding controlled for in the absence of anti-P2Y receptor antibody (no primary controls). Scale bars: 200 µm.

revealed the ability of human adipocytes to condition the culture medium with ∼50 nM ATP (Fig. 4A), which is likely to be an underestimation of the acutely pericellular ATP concentration. Scavenging extracellular ATP with apyrase caused a reduction in the resting level of cytoplasmic Ca^{2+} in human adipocytes (Fig. 4B). These data suggest that extracellular ATP generates intracellular Ca^{2+} tone in human adipocytes, so we explored this further by investigating whether constitutive activity of $P2Y_1$, $P2Y_2$ and $P2Y_{12}$ receptors contribute to resting cytoplasmic Ca^{2+} levels. There was some variability in the resting cytoplasmic Ca^{2+} concentration between donors, as well as in the presence of different vehicle controls [water or 0.1% dimethyl sulfoxide (DMSO)]; however, pairwise comparisons of the effect of each antagonist versus their respective vehicle control revealed that antagonism of either $P2Y_1$ or $P2Y_{12}$ had no significant effect on resting cytoplasmic Ca^{2+} (Fig. 4C,E). However, a marked significant reduction was observed following selective $P2Y_2$ receptor antagonism (Fig. 4D). In these experiments, resting cytoplasmic Ca^{2+} was reduced from ∼125 nM to 50 nM free Ca^{2+}, suggesting that constitutive $P2Y_2$ activity, but not $P2Y_1$ or $P2Y_{12}$, generates intracellular Ca^{2+} tone in human adipocytes.

Constitutive $P2Y_2$ receptor activity suppresses lipolysis via an adenylate cyclase-dependent mechanism

The lipolytic activity of adipocytes that produces free fatty acids and glycerol is under hormonal and nervous control, but also occurs in the absence of lipolytic stimuli (basal lipolysis). Basal lipolysis in adipocytes was measured as a time-dependent conditioning of culture medium with glycerol in the absence of stimulation. Under these conditions, adipocytes freely released glycerol over a 3-h period (Fig. 5). $P2Y_2$ receptor antagonism caused a significant increase in

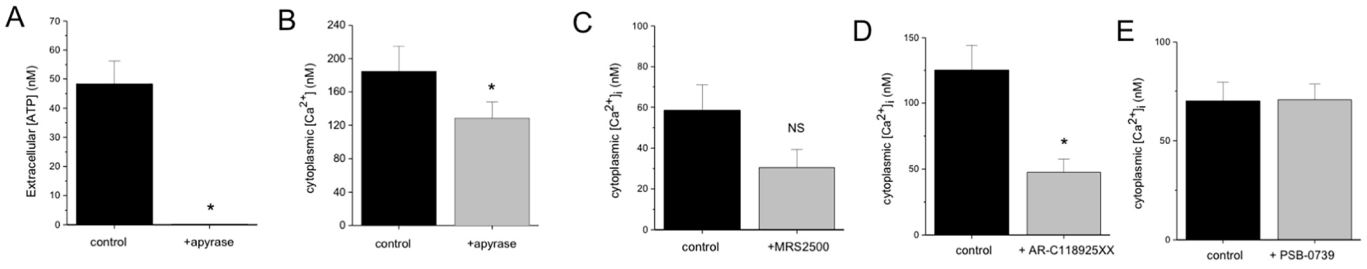

Fig. 4. Adipocyte cytoplasmic Ca^{2+} tone generated by constitutive ATP release and $P2Y_2$ receptor activation. (A) Luciferase bioluminescence measurement of extracellular ATP in culture medium conditioned by human adipocytes under control conditions and following extracellular ATP scavenging with apyrase (4 U/ml) (*N*=3). (B) Resting cytoplasmic Ca^{2+} in adipocytes in control conditions or following treatment with apyrase (4 U/ml) for 30 min (*N*=4). (C–E) Effect of P2Y receptor subtype antagonists on adipocyte resting cytoplasmic Ca^{2+}. Cells treated with MRS2500 (1 µM; $P2Y_1$) (C), AR-C118925XX (10 µM; $P2Y_2$) (D) or PSB-0739 (1 µM; $P2Y_{12}$) (E) for 30 min or vehicle (control) (*N*=6). Ca^{2+} concentrations were calculated via the calibration of the ratiometric Ca^{2+} indicator Fura-2AM. **P*<0.05 versus control throughout; NS, non-significant; *N* represents the number of donors (biological repeats).

Journal of Cell Science (2018) 131, jcs221994. doi:10.1242/jcs.221994

the rate of glycerol release, enhancing release by ~40% after 3 h (Fig. 5A). By comparison, stimulation of adipocytes with EC_{50} concentrations of isoprenaline (75 nM) to mimic nervous stimulation caused a 122±24% (N=3) increase in glycerol release versus basal conditions. The $P2Y_2$ receptor antagonist AR-C118925XX enhanced basal glycerol release in a concentration-dependent manner (Fig. 5B). To further investigate the mechanism by which $P2Y_2$ antagonism increases basal lipolysis, we quantified cellular cAMP, a positive effector of lipolysis in adipocytes, with and without AR-C118925XX treatment. AR-C118925XX treatment significantly elevated cellular cAMP in adipocytes (Fig. 5C). To support these findings, we used lentivirus delivery of short hairpin RNA (shRNA) to knock down $P2Y_2$ receptor expression in adipocytes, to investigate the impact on lipolysis and intracellular cAMP levels. Using this strategy, *$P2Y_2$* mRNA could be knocked down by 59.8±3.7% (N=5; P<0.05) versus scrambled counterparts. P2Y2 knockdown could also be observed by western blotting (Fig. S1). The rate of basal lipolysis (Fig. 5D) and intracellular cAMP levels (Fig. 5E) were both elevated in the $P2Y_2$ knockdown cells versus their scrambled counterparts. Interestingly, $P2Y_2$ knockdown adipocytes produced a small lipid droplet phenotype compared with their scrambled counterparts (Fig. 5F), and the number of droplets per cell was significantly increased (Fig. 5G). Such phenotypic changes in lipid droplets are associated with increased lipid metabolism (Paar et al., 2012). To this end, we quantified the amount of neutral lipid stored within scrambled and $P2Y_2$ knockdown adipocytes using boron-dipyrromethene (BODIPY) fluorescence, and demonstrated that $P2Y_2$ knockdown cells contained less neutral lipid (Fig. 5H). Taken together, these data suggest that reducing $P2Y_2$ activity by means of pharmacological antagonism or gene knockdown increases basal lipolysis in human adipocytes. In control experiments, antagonism of either $P2Y_1$ (Fig. 5I) or $P2Y_{12}$ (Fig. 5J) did not affect the rate of basal lipolysis, which is in line with a lack of effect on resting cytoplasmic Ca^{2+} (Fig. 4).

To further understand how inhibition of constitutive $P2Y_2$ receptor activity leads to an increase in cAMP and basal lipolysis, we examined the dependency of these effects on the activity of phosphodiesterases (PDEs) and adenylate cyclase. An elevation in intracellular Ca^{2+} is known to produce an anti-lipolytic effect in adipocytes, which has previously been ascribed to activation of Ca^{2+}-sensitive PDE subtypes (Xue et al., 2001). If the underlying mechanism through which inhibition of constitutive $P2Y_2$ activity leads to increased intracellular cAMP and enhanced lipolysis is via reducing cytoplasmic Ca^{2+} and PDE activity, it would be expected that enhanced lipolysis produced by $P2Y_2$ antagonism would be abolished by PDE inhibition. The pan-PDE inhibitor 3-isobutyl-1-methylxanthine (IBMX) increased basal lipolysis to a level comparable to that of AR-C118925XX (Fig. 6A). In addition, using subtype-specific antagonists, we observed that inhibition of PDE3 (cilostamide) and PDE4 (rolipram), but not PDE1 (vinpocetine), PDE2 (PF-05180999) or PDE7 (BRL50481), increased basal lipolysis (Fig. 6A). Cilostamide enhanced lipolysis to a level beyond that of rolipram, and is consistent with a dominant role of PDE3 in human adipocytes (Snyder et al., 2005). Combining AR-C118925XX with either cilostamide or rolipram produced a synergistic enhancement of basal lipolysis (Fig. 6A), suggesting that the effect of $P2Y_2$ antagonism on basal lipolysis is not dependent on the activity of either PDE3 or PDE4. Therefore, we looked for an alternative mechanism and explored the dependency of adenylate cyclase itself in mediating the effects of $P2Y_2$ antagonism on cAMP and basal lipolysis. By RT-PCR analysis, we identified that human adipocytes express adenylate cyclase isoforms 1–8, but not 9 (Fig. 6B). Of these isoforms, 5 and 6 are negatively regulated by cytoplasmic Ca^{2+} (Halls and Cooper, 2011) and can be selectively inhibited over other isoforms by low concentrations of SQ22536 (<10 µM) (Brand et al., 2013). Under these conditions, 1 µM SQ22536 had no significant effect on basal lipolysis (Fig. 6C), consistent with tonic suppression of adenylate cyclase, but 1 µM SQ22536 could inhibit the ability of $P2Y_2$ antagonism, with

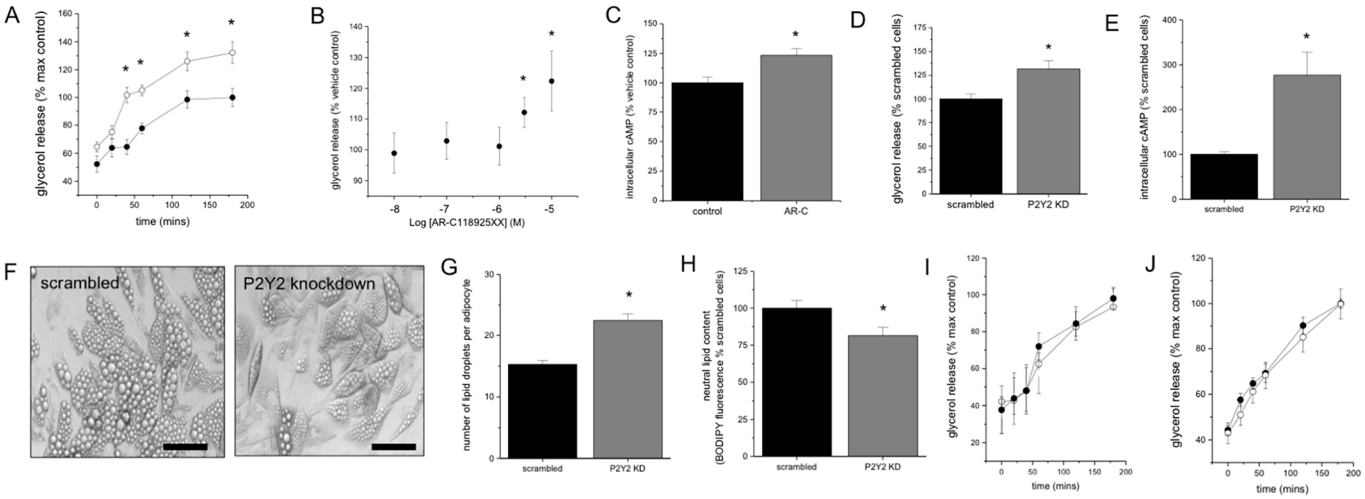

Fig. 5. $P2Y_2$ receptor antagonism or knockdown enhances basal lipolysis in human adipocytes. (A) Basal lipolysis measured in adipocytes in culture by glycerol release. Adipocytes are in the presence of vehicle (closed circles) or with $P2Y_2$ antagonist (AR-C118925XX, 10 µM; open circles) (N=3). (B) Concentration-dependent enhancement of basal lipolysis by AR-C118925XX. Data shown are glycerol release after 3 h as a percentage of vehicle control (N=3). (C) Change in intracellular cAMP in response to $P2Y_2$ antagonism (AR-C118925XX, 10 µM; 45 min) over vehicle control (N=4). (D) Change in basal lipolysis following shRNA-mediated $P2Y_2$ receptor knockdown in adipocytes versus scrambled counterparts (N=3). Glycerol release measured for 3 h. (E) Change in intracellular cAMP in $P2Y_2$ receptor knockdown adipocytes versus scrambled counterparts (N=3). (F) Representative (N=12) brightfield images to illustrate the small lipid droplet phenotype observed in $P2Y_2$ receptor knockdown adipocytes versus scrambled counterparts. Scale bars: 50 µm. (G,H) Quantitation of number of lipid droplets (N=12) (G) and neutral lipid content (BODIPY fluorescence; N=6) (H) in $P2Y_2$ receptor knockdown adipocyte versus scrambled counterparts. (I,J) Lack of effect of $P2Y_1$ receptor (MRS2500, 1 µM; open circles; N=3) (I) or $P2Y_{12}$ receptor (PSB-0739, 3 µM; open circles; N=5) (J) antagonism on basal lipolysis. *P<0.05 versus control throughout; NS, non-significant; N represents the number of donors (biological repeats).

Journal of Cell Science (2018) 131, jcs221994. doi:10.1242/jcs.221994

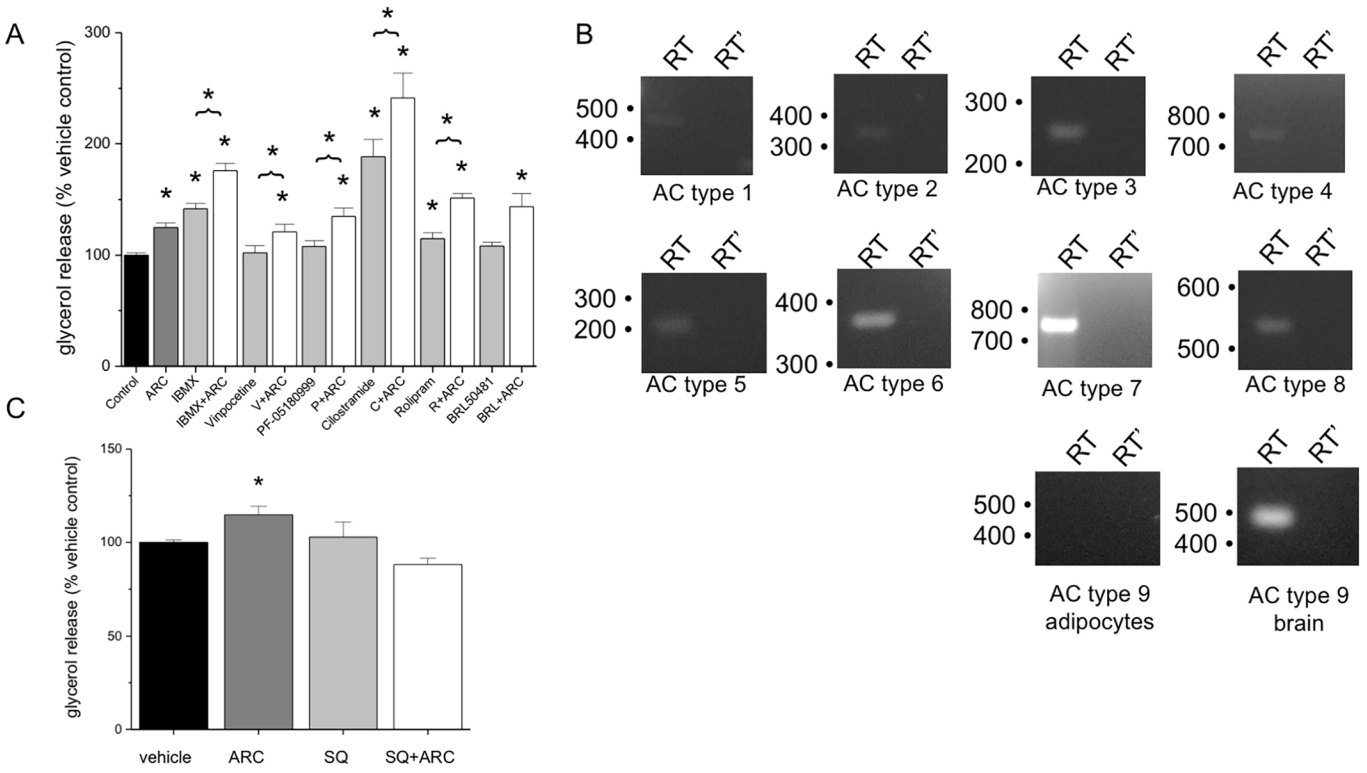

Fig. 6. $P2Y_2$ receptor antagonism synergises with phosphodiesterase inhibition, but is dependent on adenylate cyclase activity in enhancing basal lipolysis in human adipocytes. (A) Effect of antagonising phosphodiesterase (PDE) isoforms on basal lipolysis with and without $P2Y_2$ antagonism. $P2Y_2$ [AR-C118925XX (ARC); 10 µM], IBMX (pan PDE inhibitor; 10 µM), vinpocetine (PDE1; 10 µM), PF-05180999 (PDE2; 10 µM), cilostamide (PDE3; 1 µM), rolipram (PDE4; 10 µM) and BRL50481 (PDE7; 1 µM) (*N*=3). Glycerol release after 3 h expressed as a percentage of vehicle control. (B) RT-PCR detection of adenylate cyclase isoforms in human adipocytes. Expected product sizes of adenylate cyclase (AC) type 1 (446 bp), type 2 (369 bp), type 3 (263 bp), type 4 (753 bp), type 5 (202 bp), type 6 (380 bp), type 7 (746 bp), type 8 (543 bp) and type 9 (497 bp). 'brain' denotes the positive control for AC type 9 expression. 'RT'' denotes the absence of reverse transcriptase (RT; negative control for genomic DNA). (C) Effect of $P2Y_2$ receptor antagonism (ARC; 10 µM) on basal lipolysis is reversed following AC inhibition [SQ22536 (SQ); 1 µM] (*N*=6). Basal lipolysis is measured as glycerol release over 3 h in all experiments. Antagonists were added 30 min prior to the start of the assay. **P*<0.05 versus control throughout; *N* represents the number of donors (biological repeats).

AR-C118925XX, to enhance basal lipolysis in adipocytes (Fig. 6C). These data suggest that the effects of $P2Y_2$ antagonism on basal lipolysis are due to activation of Ca^{2+}-sensitive isoforms of adenylate cyclase.

Pharmacological antagonism of $P2Y_2$ leads to acute enhancement of lipolysis. However, we observed that the rate of basal lipolysis is diminished 24 h after AR-C118925XX treatment compared with counterpart cells treated with vehicle control (Fig. 7A). We reasoned that the increase in basal lipolysis might give rise to initiation of a negative feedback effect due to the enhanced secretion of adipokines with anti-lipolytic activity. To this end, we investigated the impact of pharmacological manipulation of constitutive $P2Y_2$ activity on the profile of secreted adipokines in human adipocytes. Analysis of secreted adipokines by protein array revealed changes in the profile of adipokines secreted in response to AR-C118925XX treatment (Fig. 7B; Table S2). Of particular interest was the dramatically enhanced secretion of adipokines with anti-lipolytic activity, including adiponectin (Qiao et al., 2011; Wedellová et al., 2011) and adipsin (Van Harmelen et al., 1999; Ronti et al., 2006), and the downregulation of several adipokines that stimulate lipolysis, including angiopoietin-like 4 (ANGPTL4) protein (Gray et al., 2012; La Paglia et al., 2017) and retinol-binding protein 4 (Lee et al., 2016) (Fig. 7C).

DISCUSSION

This study has identified a diverse profile of purinergic receptors present in primary human adipocytes; however, interestingly, only $P2Y_1$, $P2Y_2$ and $P2Y_{12}$ receptors appear to be functionally involved in nucleotide-evoked Ca^{2+} responses. Although $P2X_{4\text{-}7}$ receptors were detected at both the mRNA and protein level, the ATP response appears to be mediated by metabotropic P2Y receptors, as evidenced by the persistence of response in the absence of extracellular Ca^{2+}, abolishment of the response when PLC was inhibited, and no effect of selective antagonism of $P2X_4$ and $P2X_7$. $P2X_4$ receptors are known to localise to lysosomes and rapidly traffic to and from the plasma membrane in other cell types (Stokes, 2013; Ashour and Deuchars, 2004), which might explain why exogenous application of ATP was unable to activate $P2X_4$. A lack of involvement of $P2X_5$ and $P2X_6$ is unsurprising, as these receptors are not functional in humans (Torres et al., 1999; Ormond, 2006; Kotnis et al., 2010). $P2X_7$ receptors require very high concentrations of ATP to be activated (North, 2002), so perhaps in this study, the concentration of ATP used was not sufficiently elevated to activate $P2X_7$. In addition, several P2Y receptor subtypes ($P2Y_4$, $P2Y_6$, $P2Y_{11}$ and $P2Y_{13}$) were also detected in human adipocytes, but do not appear to play a functional role in nucleotide-evoked Ca^{2+} responses in these cells. In the case of $P2Y_4$, it is not possible to definitively rule out a role for this receptor, due to the absence of a commercially available selective antagonist for $P2Y_4$ (Jacobson et al., 2009). However, the observation that the response to UTP, the preferred agonist for $P2Y_4$, is abolished by selective antagonism of $P2Y_2$ indicates that $P2Y_4$ is unlikely to play a role in the UTP-evoked Ca^{2+} response in human adipocytes. A possible explanation

Journal of Cell Science (2018) 131, jcs221994. doi:10.1242/jcs.221994

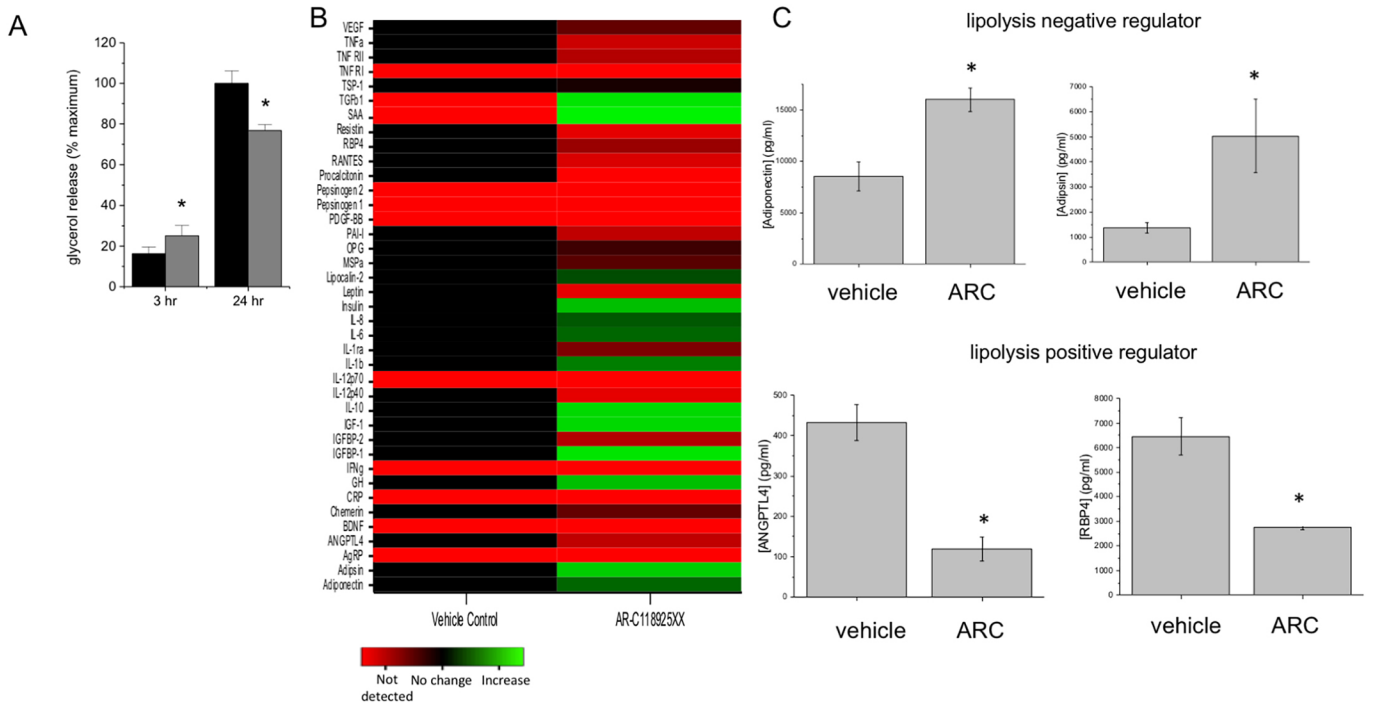

Fig. 7. Longer-term suppression of basal lipolysis in human adipocytes following $P2Y_2$ receptor antagonism is associated with an anti-lipolytic adipokine profile. (A) Glycerol release (basal lipolysis) measured 3 h and 24 h after singular exposure to vehicle (black bars) or $P2Y_2$ antagonist (AR-C118925XX, 10 µM; grey bars) (*N*=4). (B) Heat map representing average change in secreted adipokines 24 h after adipocyte exposure to vehicle or 10 µM AR-C118925XX (*N*=4), as determined by quantitative protein array. Fold changes are expressed relative to levels of secreted adipokines before exposure to vehicle or AR-C118925XX. (C) Bar charts showing significant increases in adiponectin and adipsin (negative regulators of lipolysis), and decrease in ANGPTL4 and RBP4 (positive regulators of lipolysis), to illustrate the shift to an anti-lipolytic adipokine profile 24 h after adipocyte singular exposure to 10 µM AR-C118925XX (ARC; *N*=4). **P*<0.05 versus control. *N* represents the number of donors (biological repeats).

for the lack of involvement of $P2Y_4$, $P2Y_6$, $P2Y_{11}$ and $P2Y_{13}$ receptors is that $P2Y_2$ receptor activation caused heterologous desensitisation of these subtypes (Govindan and Taylor, 2012). An important caveat to this study is that the Ca^{2+} responses reported are measurements from populations of adipocytes, and therefore variability of responses at the single-cell level will be lost.

The $P2Y_2$ receptor is capable of sensing extracellular ATP in the nanomolar range (Lazarowski et al., 1995), thus the concentration of extracellular ATP released by adipocytes in this study is sufficient to activate $P2Y_2$. Here, we report that these properties of the $P2Y_2$ receptor allow it to be constitutively active due to the extracellular ATP microenvironment of human adipocytes. Furthermore, we provide data to demonstrate the functional importance of this constitutive activity in regulation of adipocyte intracellular Ca^{2+} tone, the rate of basal lipolysis and the profile of secreted adipokines. Although this is the first demonstration in human adipocytes, we and others have previously demonstrated the role purinergic receptors can play in autocrine regulation of mammalian cells due to constitutive or agonist-triggered ATP release (Corriden and Insel, 2010; Sivaramakrishnan et al., 2012).

In this study, we contribute the acute anti-lipolytic activity of $P2Y_2$ antagonism to a decrease in resting cytoplasmic Ca^{2+}. Previous studies have highlighted an importance of free cytoplasmic Ca^{2+} in regulating lipolysis (Xue et al., 2001), although the molecular mechanisms underlying this are unclear. Certain PDE isoforms, specifically PDE1 isoforms, are sensitive to and activated by Ca^{2+} (Omori and Kotera, 2007) via a Ca^{2+}/calmodulin-dependent mechanism. Stimulation of basal lipolysis following $P2Y_2$ antagonism could arise via this mechanism due to a decrease in cytoplasmic Ca^{2+} and the consequent loss of PDE activity, increasing the availability of cAMP and promoting lipolysis. However, our findings do not support this mechanism as direct PDE inhibition has a synergistic effect with $P2Y_2$ antagonism on lipolysis. Furthermore, use of the vinpocetine, a selective inhibitor of Ca^{2+}/calmodulin-sensitive PDE1 isoforms, had no effect on basal lipolysis, suggesting that PDE1 does not regulate basal lipolysis. As the stimulatory action of $P2Y_2$ receptor antagonism on basal lipolysis is completely inhibited by the adenylate cyclase inhibitor SQ22536, we suggest that the role of constitutively active $P2Y_2$ might be to directly control the activity of adenylate cyclase and acutely regulate lipolysis via this route. One interesting observation is that adenylate cyclase inhibition does not decrease basal lipolysis, which suggests that adenylate cyclase activity is tonically suppressed. This observation is consistent with findings in rodent adipocytes (Juan et al., 2005; Jun et al., 2006). Our model suggests that adenylate cyclase activity does not contribute to the basal lipolytic capacity of adipocytes due to tonic suppression by elevated cytoplasmic Ca^{2+} (Fig. 8). However, basal lipolysis occurs even in the absence of adenylate cyclase activity or activation of hormone-sensitive lipase (HSL) via the cAMP/PKA signalling axis, which is a known and important mediator of hormone and nervous stimulated lipolysis. This can be explained by the existence of ATGL, which is a cAMP-independent lipase known to regulate basal lipolysis (Miyoshi et al., 2008; Wang et al., 2011).

The correlation between $P2Y_2$ receptor activity, elevated intracellular Ca^{2+}, cAMP reduction and lowered basal lipolysis, has led us to hypothesise that constitutive $P2Y_2$ activity suppresses adenylate cyclase activity (Fig. 8). There is precedence for a role for adipocyte cytoplasmic Ca^{2+} tone in regulating adenylate cyclase activity, as several adenylate cyclase isoforms (types 5 and 6) are Ca^{2+} sensitive (Cioffi et al., 2002). Type 6, in particular, has been

Journal of Cell Science (2018) 131, jcs221994. doi:10.1242/jcs.221994

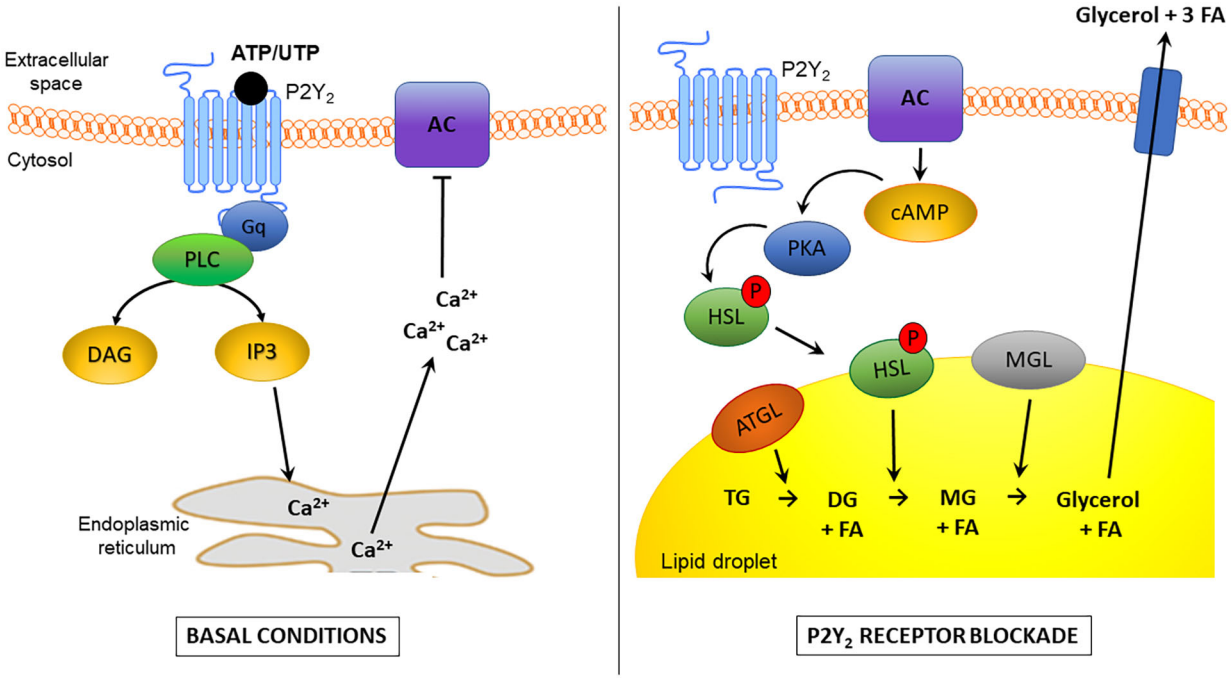

Fig. 8. Schematic diagram of the proposed mechanism by which $P2Y_2$ receptor activation causes acute suppression of lipolysis in primary human *in vitro*-differentiated adipocytes. Under basal conditions (left), $P2Y_2$ receptors are activated by ATP or UTP released by the adipocytes into the extracellular space, which the subsequently activates a Gq heterotrimeric G-protein and phospholipase C (PLC)-mediated production of diacylglycerol (DAG) and inositol triphosphate (IP3). The IP3 then binds to receptors on the surface of the endoplasmic reticulum to initiate the release of Ca^{2+} from the endoplasmic reticulum into the cytosol. This elevation of cytoplasmic Ca^{2+} causes tonic inhibition of Ca^{2+}-sensitive adenylate cyclase (AC) isoforms. However, in the absence of $P2Y_2$-receptor mediated inhibition of AC due to blockade of $P2Y_2$ receptor signalling (right), intracellular Ca^{2+} concentrations are lower, and therefore AC is not inhibited and consequently free to convert ATP to cyclic AMP (cAMP). The increase in intracellular cAMP activates protein kinase A (PKA), which is then able to phosphorylate cytoplasmic hormone-sensitive lipase (HSL). This allows HSL to translocate the lipid droplet. Here, adipose triglyceride lipase (ATGL) catalyses the hydrolysis of triglycerides (TG) to diglycerides (DG) and a free fatty acid (FA) molecule, then HSL catalyses the conversion of DG to monoglycerides (MG) and FA, and finally monoglyceride lipase (MGL) catalyses the lipolytic breakdown of MG to glycerol and FA. The glycerol and three FA molecules can then be transported out of the cell and released into the bloodstream, where they can travel to the liver or other organs to be utilised as an energy source.

shown to be inhibited by Ca^{2+} entry through store-operated channels, which are likely to be opened following $P2Y_2$ receptor activation. The molecular basis of some of these channels has recently been identified in mouse adipocytes, where they control adiponectin secretion (Sukumar et al., 2012).

Here, we demonstrate that pharmacological inhibition of $P2Y_2$ has a biphasic effect on lipolysis, an acute stimulatory effect (within 3 h) followed by a reduction in lipolysis after 24 h. The consequent reduction could be the result of a change in the profile of secreted adipokines following $P2Y_2$ antagonism. Adipocytes can sense and autoregulate their lipolytic capacity through autocrine adipokine signalling. There is evidence for a local negative-feedback loop between increased lipolysis and the release of adiponectin, whereby elevated free fatty acid concentrations promote adiponectin secretion (Bernstein et al., 2004; Krzyzanowska et al., 2007), which, in turn, acts on adipocytes to inhibit lipolysis (Qiao et al., 2011). There is a clear link between increased adipocyte metabolism and adipocyte inflammation (Greenberg and Obin, 2006). In obesity, the well-documented recruitment of macrophages into adipose tissue and decreased insulin sensitivity is likely to underlie the enhanced basal lipolysis in inflamed adipose tissue (Weisberg et al., 2003), although some inflammatory cytokines also have acute actions on adipose function (Zhang et al., 2002). It is interesting, therefore, that antagonism of $P2Y_2$ leads to enhance secretion of several inflammatory cytokines, including TGF-β and IL-8, and markers of acute-phase inflammation including serum amyloid A and plasminogen activator inhibitor-1. Such factors may be secreted in response to the acute increase in lipolysis following AR-C118925XX treatment.

In summary, we provide evidence that constitutive $P2Y_2$ activity is important for the regulation of basal lipolysis. We also demonstrate that perturbations in its activity and consequent enhanced basal lipolysis alter the profile of secreted adipokines in human *in vitro*-differentiated adipocytes. This study highlights the $P2Y_2$ receptor and micro-environmental ATP as novel targets for pharmacological manipulation of WAT function.

MATERIALS AND METHODS

Chemicals and reagents

All chemicals were purchased from Sigma-Aldrich (Dorset, UK) unless otherwise stated. Selective antagonists were obtained from Tocris Bioscience (Bristol, UK) ($P2Y_1$, MRS2500; $P2Y_2$, AR-C118925XX; $P2Y_6$, MRS2578; $P2Y_{11}$, NF340; $P2Y_{12}$, PSB-0739; $P2Y_{13}$, MRS2211; $P2X_4$, PSB12062; $P2X_7$, A438079; adenylate cyclase, SQ22536; G_i signalling, pertussis toxin). U73122 (phospholipase C) was purchased from Santa Cruz Biotechnology (Texas, DA, USA). All isoform-selective PDE inhibitors (PDE1, vinpocetine; PDE2, PF-05180999; PDE3, cilostamide; PDE4, rolipram; PDE7, BRL50481) were purchased from Sigma-Aldrich. Nucleotides were purchased from Abcam (Cambridge, UK), excluding ADP and UDP (Sigma-Aldrich).

Tissue donation

Subcutaneous abdominal adipose tissue samples were obtained from 48 healthy female volunteers, with an average age of 55.5±1.5 (*N*=45, range 38–75), undergoing elective delayed deep inferior epigastric

perforator flap operations. All recruited patients were prior breast cancer sufferers who have had mastectomies as part of their cancer treatment and are now in remission. Recruited patients had an average body mass index (BMI) value of 27.7±0.5 (N=34, range 24–35). Patients were normotensive with an average mean arterial pressure of 98.4±1.6 (N=44). Samples were obtained with the assistance of the plastic surgery team at the Norfolk and Norwich University Hospital (NNUH). All volunteers were screened to exclude diabetics, patients with infections or cancer, and patients on anti-inflammatory medication. Informed written consent was obtained from all volunteers prior to participation in the study. This study was ethically approved by the London-Stanmore Research Ethics Committee (152093) and the Research and Development department at the NNUH (2014EC03L).

Primary cell isolation from adipose tissue and *in vitro* differentiation

Primary cells were isolated from human subcutaneous adipose tissue using a slightly adapted form of standard isolation procedures (Turner et al., 2010). In brief, fresh adipose tissue samples were dissected to remove blood vessels, fibrous tissue and skin. The samples were then further minced and enzymatically digested with collagenase (type 1A) from *Clostridium histolyticum* (Sigma-Aldrich) and bovine pancreatic DNase I (Biomatik, Cambridge, Canada) for 30 min at 37°C with regular mixing by inversion. The digested tissue samples were then passed through a 70 µm cell strainer and centrifuged for 5 min at 450 ***g***, which separated the sample into a floating fraction containing mature adipocytes and a pellet containing multipotent mesenchymal stromal cells (MSCs). The adipocytes were discarded and the MSCs were treated with a red cell lysis buffer, washed and then resuspended in culture medium [Dulbecco's modified Eagle medium (DMEM) supplemented with 4.5 g/l glucose, sodium pyruvate, L-glutamine, 10% fetal bovine serum (FBS) (v/v), 50 IU/ml penicillin and 50 µg/ml streptomycin] and left in a T175 flask overnight in a humidified incubator at 37°C with 5% CO_2. The following day, the cells were washed twice with PBS to remove any non-adherent cells or debris, and left in fresh serum-containing medium until the cells were confluent, at which point they were trypsinised and seeded for experimental use. In this study, MSCs were plated at an initial seeding density of 2×10^4 cells/well in 96-well plates, unless otherwise indicated. The cells were then allowed to grow to hyperconfluence over the next 4 days and then the differentiation protocol was initiated by removing the culture medium and replacing it with differentiation medium – which consisted of DMEM supplemented with 10% FBS, 50 IU/ml penicillin, 50 µg/ml streptomycin, 0.2 mM indomethacin, 1 µM dexamethasone, 0.5 mM IBMX and 100 nM insulin – for 14 days. The differentiation medium was replaced every 4 days. After 2 weeks, the differentiation medium was removed and exchanged back to culture medium for a further 3 days before experimental use to allow the cells to habituate. In all instances in which adipocytes are mentioned in this study, they are cells that have undergone the full *in vitro* differentiation and habituation protocol described. MSCs were passaged a maximum of four times for differentiation, although the majority of experiments were performed using cells from passage 1 and 2. Only cells that displayed >90% differentiated cells (as judged by eye) were deemed adequate for experimental use. All experiments were performed using cells from at least three independent donors.

Calcium mobilisation experiments

Culture medium was aspirated off *in vitro*-differentiated adipocytes and the cells were gently washed with salt buffered solution (SBS) (pH 7.4), containing 130 mM NaCl, 5 mM KCl, 1.2 mM $MgCl_2$, 1.5 mM $CaCl_2$, 8 mM D-(+)-glucose and 10 mM HEPES. The cells were then loaded with 2 µM Fura-2AM (Abcam) in SBS supplemented with 0.01% (w/v) pluronic for 1 h at 37°C while being protected from light. The loading buffer was then removed and the cells were washed twice with SBS. Where applicable, the cells were incubated for a further 30 min with vehicle/antagonists or Ca^{2+}-free SBS (SBS lacking 1.5 mM $CaCl_2$, but containing 2 mM EGTA, pH 7.4). For pertussis toxin experiments, the pertussis toxin was added to the culture medium 4 h prior to commencing the Ca^{2+} mobilisation experiments. All antagonists were dissolved in water or DMSO and were then further diluted in SBS, so that a final concentration of 0.1% DMSO was not exceeded, excluding U73122 and MRS2578, which required a final concentration of 1% DMSO. Finally, the cells were maintained at 37°C and challenged with nucleotides administered by a FlexStation III microplate reader (Molecular Devices, San Jose, CA, USA), which also recorded the fluorescence (excitation 340 nm and 380 nm, emission 510 nm) every 3 s to provide fluorescence ratio (F_{ratio}) values. F_{ratio} values at every time point, peak F_{ratio} and area under the curve data were extracted using SoftMax Pro 5.4.5 (Molecular Devices) software.

Calcium calibration

In vitro-differentiated adipocytes were loaded with Fura-2AM as per the Ca^{2+} mobilisation experiment protocol and then incubated with SBS or Ca^{2+}-free SBS for 30 min at 37°C, prior to challenging the cells with 2 µM ionomycin and recording the changes in intracellular Ca^{2+} levels using a Flexstation III microplate reader. The Grynkiewicz formula (Grynkiewicz et al., 1985) was then utilised to convert F_{ratio} values from Ca^{2+} mobilisation assays to intracellular Ca^{2+} concentrations. The Grynkiewicz formula is as follows:

$$[Ca^{2+}]_i = K_D \times \beta \times (R-R_{min})/(R_{max}-R)$$

where K_D is the K_D for Fura2-AM at 37°C, which is 224 nM; β is the maximum fluorescence intensity at 380 nm for ionomycin in the absence of Ca^{2+}, divided by the minimum fluorescence at 380 nm for ionomycin in the presence of Ca^{2+}; R_{min} is the minimum F_{ratio} value for ionomycin in the absence of Ca^{2+}; R_{max} is the maximum F_{ratio} value for ionomycin in the presence of Ca^{2+}; and R is the F_{ratio} value that needs to be converted. β, R_{max} and R_{min} were calculated by averaging the data from three independent donors.

Immunocytochemistry

MSCs were seeded onto glass coverslips and differentiated *in vitro*. All subsequent steps were conducted at room temperature, unless otherwise stated. Culture medium was gently aspirated off the cells and the cells were washed with PBS, fixed with 4% paraformaldehyde for 15 min and then permeabilised with 0.25% Triton X-100 for 10 min. Non-specific binding was blocked with 1% bovine serum albumin (BSA), and the cells were then incubated with the appropriate primary antibody (1:200) overnight at 4°C. Primary antibodies were purchased from Santa Cruz Biotechnology (P2X5, sc-15192, RRID:AB_2158092; $P2Y_{12}$, sc-27152, RRID:AB_2155964), Alomone Labs (Jerusalem, Israel) (P2X4, APR-002, RRID:AB_2040058; P2X7, APR-004, RRID:AB_2040068; $P2Y_1$, APR-009, RRID:AB_2040070; $P2Y_4$, APR-006, RRID:AB_2040080; $P2Y_6$, APR-011, RRID:AB_2040082; $P2Y_{11}$, APR-015; $P2Y_{13}$, APR-015, RRID:AB_2040072) and Abcam ($P2Y_2$, ab10270, RRID:AB_297008). All antibodies used were polyclonal and raised in rabbits, excluding those purchased from Santa Cruz Biotechnology, which were raised in goats. Excess primary antibody was removed and successful binding was detected using rabbit anti-goat (Abcam) or goat anti-rabbit (Thermo Fisher Scientific, Waltham, MA, USA) Alexa Fluor 488-conjugated secondary antibodies (1:1000 dilution). Finally, cells were mounted using VectaShield-containing 1.5 µg/ml 4′,6-diamidino-2-phenylindole (DAPI; Vector Laboratories, Peterborough, UK) and imaged using a Zeiss confocal microscope.

Immunohistochemistry

Fresh human subcutaneous adipose tissue was cut into 1 cm^2 pieces and washed with PBS to remove excess blood. Next, the tissue was submerged in 4% ice-cold paraformaldehyde for 4 h, then washed with PBS for 30 min twice and left in PBS overnight at 4°C. The tissue was then sequentially submerged in increasing concentrations of ethanol (30, 50, 70, 90, 95, 100% and 100%) for 1 h each for dehydration, then submerged in histo-clear (National Diagnostic, Atlanta, GA, USA) for 1 h and embedded in paraffin. For paraffin embedding, the tissue was placed in molten paraffin for 2 h twice, and then the embedded tissue was placed in a mould and encased in paraffin. The paraffin-embedded tissue was left overnight at 4°C to set, and subsequently cut into 6 µm sections using a Microm HM355S

automatic microtome (Thermo Fisher Scientific) and mounted onto (3-aminopropyl)triethoxysilane-coated glass slides. When the slides were dry, the sections were dewaxed with histo-clear (5 min twice) and rehydrated by sequentially submerging in decreasing concentrations of ethanol (100, 95, 80, 70, 50 and 30% for 1 min each), followed by distilled water for 1 min. The dewaxed sections were then stained using an anti-rabbit or anti-goat HRP-DAB Cell & Tissue Staining Kit purchased from R&D Systems (Minneapolis, MN, USA) as per the manufacturer's instructions. The sections were incubated with primary antibodies for $P2Y_1$ (sc-20123, RRID:AB_2158393), $P2Y_2$ (sc-20124, RRID:AB_2156139) or $P2Y_{12}$ (sc-27152, RRID:AB_2155964) (1:200 in PBS with 1% BSA), or PBS with 1% BSA alone, overnight at 4°C. All primary antibodies were purchased from Santa Cruz Biotechnology. When the staining protocol was complete, the sections were dehydrated again by rapidly dipping the slides in increasing concentrations of ethanol, and then histo-clear for 10 min, and finally mounted in DPX mountant. Once the mountant was dry, images of stained sections and no primary antibody controls were taken using a CKX41 inverted microscope (Olympus, Tokyo, Japan).

RNA extraction and cDNA synthesis

In vitro-differentiated adipocytes were lysed with TRI-reagent and then treated with 100 µl 1-bromo-3-chloropropane and centrifuged to partition the sample. The top aqueous phase was then carefully transferred into a fresh tube and the RNA was precipitated with isopropanol and washed with 75% ethanol. The RNA was centrifuged at 12,000 ***g*** for 10 min, the supernatant was removed and the RNA pellet was air-dried. The RNA was then resuspended in molecular-grade water and potential genomic DNA contamination was removed using a DNA-free™ DNA Removal Kit (Thermo Fisher Scientific) as per the manufacturer's instructions. The purity and quantity of RNA was assessed using a Nanodrop 2000 (Thermo Scientific, Wilmington, DE, USA).

For each sample, 500 ng RNA was primed with 100 ng random hexamer primers (Bioline, Taunton, MA, USA) by heating the mixture to 70°C for 10 min. Each sample was then incubated with 250 µM dNTPs (Bioline), 30 U RNasin ribonuclease inhibitor (Promega, Madison, WI, USA), 0.01 M dithiothreitol, first-strand buffer and 200 U Superscript III Reverse Transcriptase (RT) (Thermo Fisher Scientific) for 1 h at 42°C. A duplicate sample with no RT was run alongside as a control for genomic DNA contamination. The PCR reaction was terminated by heating the samples to 70°C for 10 min. Complementary DNA (cDNA) samples were then stored at −20°C.

Quantitative RT-PCR

The cDNA and their corresponding no RT controls were diluted to 2 ng/µl and mixed with TaqMan™ Fast Universal PCR Master Mix (Thermo Fisher Scientific). Commercially available TaqMan gene expression assay primers and probes for each gene of interest (GOI) were also added (*$P2Y_1$*, Hs00704965_s1; *$P2Y_2$*, Hs04176264_s1; *$P2Y_4$*, Hs00267404_s1; *$P2Y_6$*, Hs00366312_m1; *$P2Y_{11}$*, Hs01038858_m1; *$P2Y_{12}$*, Hs01881698_s1; *$P2Y_{13}$*, Hs03043902_s1; *$P2Y_{14}$*, Hs01848195_s1; *$P2X_1$*, Hs00175686_m1; *$P2X_2$*, Hs04176268_g1; *$P2X_3$*, Hs01125554_m1; *$P2X_4$*, Hs00602442_m1; *$P2X_5$*, Hs01112471_m1; *$P2X_6$*, Hs01003997_m1; *$P2X_7$*, Hs00175721_m1; *RPLP0*, Hs99999902_m1). Each sample was then amplified in a MicroAmp fast optical 96-well reaction plate on an Applied Biosystems 7500 Real-Time PCR System (Thermo Fisher Scientific) for 40 cycles. Threshold cycle (C_T) values were extracted from the 7500 software v2.0.6. Receptors with C_T values below 35 were deemed to be expressed. Ribosomal protein lateral stalk subunit P0 (*RPLP0*) was used as an endogenous control to normalise for any variability in cDNA template input.

RT-PCR

cDNA (or no RT control sample) (1 µg) was mixed with 25 µl ReadyMix™ Taq PCR Reaction Mix, 0.2 µM forward primers, 0.2 µM reverse primers and water to achieve a total volume of 50 µl. The following PCR conditions were employed for each GOI: initial denaturation at 94°C for 1 min, then 35 cycles of 94°C for 30 s, variable annealing conditions according to GOI and 72°C for 1 min, followed by 5 min at 72°C for the final extension. The annealing conditions were 55°C for 30 s for all primer sequences, excluding adenylate cyclase types 2, 3, 8 and 9, which had an annealing temperature of 52°C (1 min) and adenylate cyclase type 7, which had an annealing temperature of 45°C (1 min). Primer sets used for adenylate cyclase types were as follows: type 1, sense 5′-CATGACCTGCGAGGACGAT-3′, anti-sense 5′-ACAGGAGACTGCGAATCTGAA-3′; type 2, sense 5′-GGGGC-TGCGTTTCTCT-3′, anti-sense 5′-CAGGAACACGGAACAGGATA-3′; type 3, sense 5′-CACGGGACCCAGCAAT-3′, anti-sense 5′-GCTCTAA-GGCCACCATAGGTA-3′; type 4, sense 5′-TCCAAGCTCCCAATG-TGTCC-3′, anti-sense 5′-CTTGTCCAGAGGTGGCATTT-3′; type 5, sense 5′-TCTGGTCTAACGATGTCACGC-3′, anti-sense 5′-TCTTTCC-GCTTCTGGGTGC-3′; type 6, sense 5′-GGCATTGATGATTCCAGC-AAAGAC-3′, anti-sense 5′-TGCAGGGCCTTAGGGAACAGA-3′; type 7, sense 5′-CCAGTCTGGATGCACAGGAG-3′, anti-sense 5′-AGCCTCCC-ATCAAAGAACCG-3′; type 8, sense 5′-CGGGATTTGGAACGCC-TCTA-3′, anti-sense 5′-CCGGTCTGACAGGTAACTGATAA-3′; type 9, sense 5′-CACCGCAAAATACTTAGATGACG-3′, anti-sense 5′-CCTT-CTCCTGCAAGATCTCACAC-3′.

Glycerol quantification assay

In vitro-differentiated adipocytes were washed once with PBS and then incubated with 100 µl/well DMEM (without serum or antibiotics) for 2 h at 37°C with 5% CO_2. Immediately following this incubation period, 1 µl/well vehicle or antagonist was added directly to each well and the cells were incubated for a further 30 min at 37°C with 5% CO_2. Next, a further 50 µl/well DMEM containing vehicle or agonists was added to each well. For the time series assays, a sample was collected immediately after the agonist was added by gently pipetting to mix, and then 100 µl/well supernatant was removed and placed in a fresh 96-well plate and kept on ice for the duration of the experiment. These initial samples were labelled '0 min', and then samples were taken after 20, 40, 60, 120 and 180 min had lapsed. The cells were incubated at 37°C with 5% CO_2 between sample intervals. Alternatively, for all non-time series glycerol experiments, samples were taken 3 h after vehicle/agonist was added. After the final sample was collected, all the samples were then stored at −80°C or used immediately for the glycerol quantification assay. A glycerol assay kit was purchased from Sigma-Aldrich and performed as per the manufacturer's instructions. A standard curve was run with each assay run. Owing to variation in basal glycerol levels between donors, the data were normalised to the amount of glycerol produced under the control conditions after 3 h.

ATP quantification assay

In vitro-differentiated adipocytes were washed once with PBS and then incubated with 50 µl/well DMEM (without serum or antibiotics) for 1 h at 37°C with 5% CO_2. Next, 1 µl vehicle or antagonist was added directly to each well and the cells were incubated for a further 1 h at 37°C with 5% CO_2. The supernatant was then carefully removed, taking care not to disturb the cells, and the ATP was quantified using an ATP Bioluminescence Assay Kit HS II (Roche, Mannheim, Germany) performed as per the manufacturer's instructions. A standard curve was run with each assay. An integration time of 1 s was used for the bioluminescence readings. ATP levels in cell-free culture medium in each experimental condition were quantified and subtracted from test samples. The total cell number and supernatant volume were standardised for all experiments.

Cyclic AMP quantification assay

In vitro-differentiated adipocytes were washed once with PBS and then incubated with 100 µl/well DMEM (no serum or antibiotics) for 2 h at 37°C, and then the 1 µl/well vehicle/antagonist was added to each well and the cells were incubated for a further 30 min at 37°C. DMEM alone or agonist (50 µl/well) was added to each well and the cells were incubated for a further 15 min at 37°C. The cells were then washed twice with ice-cold PBS and lysed on ice with 100 µl/well 1× cell lysis buffer containing 1 mM phenylmethylsulfonyl fluoride. The rest of the assay was performed as per the manufacturer's instructions for the Cyclic AMP XP® Assay Kit (Cell Signaling Technology, Leiden, The Netherlands).

Lentiviral shRNA knockdown

Bacterial glycerol stocks of pLKO.1 puro vectors carrying Mission® non-target shRNA control sequences or shRNA sequences that targeted the $P2Y_2$ gene (TRCN0000009481) were purchased from Sigma-Aldrich. Bacterial stocks of psPAX2 (viral packaging plasmid) and pMD2.G (viral envelope plasmid) were purchased from Addgene (Cambridge, MA, USA). HEK239/17 cells (American Type Culture Collection, CRL-11268, RRID:CVCL 1926) were transfected with 12 µg psPAX2, 3 µg pMD2.G and 9 µg non-target shRNA control plasmid DNA (scrambled control) or plasmid DNA containing shRNA targeting $P2Y_2$ ($P2Y_2$ shRNA), in the presence of Lipofectamine™ 2000 (Thermo Fisher Scientific). The HEK293/17 cells were grown in normal culture medium (DMEM with 10% FBS and 1% antibiotics) and this was exchanged for 20 ml viral collection medium (DMEM supplemented with 1% FBS and no antibiotics) immediately before adding the plasmid DNA and lipofectamine, which was diluted in 1.2 ml OPTI-MEM medium (Thermo Fisher Scientific), drop-wise to the cells. The cells were then incubated for 6 h with this mixture at 37°C in 5% CO_2. The medium was then replaced with fresh viral collection medium and then cells were left to incubate at 37°C in 5% CO_2 for 72 h, with the medium being collected (and stored at 4°C) and replaced with fresh viral collection medium every 24 h. After 72 h had lapsed, the virus-containing medium was passed through a 0.45 µm filter to remove cell debris, and then the virus was concentrated using Lenti-X concentrator solution (Clontech, Fremont, CA, USA) as per the manufacturer's instructions. The resulting concentrated virus was then aliquoted and stored at −80°C until required. A p24 ELISA was performed using a QuickTiter™ Lentivirus Titer Kit (Cell Biolabs, San Diego, CA, USA) as per the manufacturer's guidelines to calculate the multiplicity of infection (MOI) for both the scrambled control and $P2Y_2$ shRNA lentiviral particles. These values were then used to ensure that equivalent amounts of control and target lentivirus were used for subsequent experiments.

In vitro-differentiated adipocytes were washed once with PBS and 200 µl/well fresh culture medium (DMEM containing 10% FBS and antibiotics) was added to each well. Then 8 µg/ml polybrene and scrambled control or $P2Y_2$ shRNA lentiviral particles (MOI of 1000) was added to each well and the cells were incubated for 18 h at 37°C in 5% CO_2. The following day, the medium was removed and replaced with fresh culture medium and the cells were incubated for a further 4 days at 37°C in 5% CO_2 before they were ready for experimental use. Following experimental use, the cells were lysed and successful $P2Y_2$ knockdown was confirmed using quantitative RT-PCR.

BODIPY staining

In vitro-differentiated adipocytes transfected with scrambled control or $P2Y_2$ shRNA lentiviral particles were stained with BODIPY 493/503 lipid dye (Thermo Fisher Scientific) to quantitate any changes in total lipid content due to reduction of $P2Y_2$ expression. To do this, the culture medium was removed and replaced with 100 µl/well DMEM (no FBS or antibiotics) and a further 100 µl/well of DMEM containing 2 µM BODIPY 493/503 dye was added and immediately mixed thoroughly by gently pipetting. The cells were then incubated for 30 min at 37°C in the dark. The excess dye was then removed and the cells were washed twice with PBS, and then the fluorescence at 493/503 nm (excitation/emission) was measured using a Flexstation III microplate reader. Each experiment was normalised for background fluorescence, by measuring and subtracting the fluorescence values for cells in the absence of the dye.

Lipid droplet quantification

Images of human *in vitro*-differentiated adipocytes that had been treated with both scrambled and $P2Y_2$ shRNA lentiviral particles were taken using an Olympus CKX41 inverted microscope for 12 independent donors. These images were then anonymised to eliminate operator bias and analysed using the counter plugin on Image J (National Institutes of Health, Bethesda, MD, USA). The number of lipid droplets in 15 individual cells from each image was quantified. Once all the counting was complete, the values were sorted according to whether they were calculated from an image of scrambled or $P2Y_2$ knockdown adipocytes to perform statistical analyses.

Adipokine array

In vitro-differentiated adipocytes were washed once with PBS and then incubated with 100 µl/well DMEM (no serum or antibiotics) for 2 h at 37°C in 5% CO_2. Next, 1 µl/well vehicle or antagonist was added to each well and the cells were incubated for a further 30 min at 37°C in 5% CO_2, before the first supernatant samples were taken for the 0 h time point by gently pipetting up and down and then transferring 75 µl/well into a fresh 96-well plate. Additional samples were taken in this manner after 3 h and 24 h. All the samples were stored at −80°C until required.

A Human Obesity Array Q3, which has the capacity to detect 40 human adipokines, was purchased from RayBiotech (Norcross, GA, USA). When supernatant samples had been collected from four independent donors, the samples were defrosted and allowed to warm to room temperature before conducting the protein array. The protein array was then performed as per the manufacturer's instructions and sent back to the manufacturer for analysis. The median fluorescence values were used for adipokine quantification analysis and a heat map was generated by normalising the average adipokine concentrations to the vehicle control.

Statistical analysis

Results were analysed, including statistical analyses, using Origin Pro 2017 software (Origin Lab, Northampton, MA, USA). All concentration response data were normalised to the maximal response. In cases of variability between donors, the concentration that produced the maximum response in the majority of donors was used. Data were normalised to their respective vehicle controls. Concentration response curves were fitted by Origin using the Hill Equation. *N* applies to the number of donors throughout.

Data were assessed for normality using a Shapiro–Wilk test and then normally distributed data were assessed using a paired/unpaired Student's *t*-test or ANOVA with a post hoc Tukey test. Non-normally distributed data were assessed by paired sample Wilcoxon signed rank test, Mann–Whitney test or Kruskal–Wallis ANOVA with a post hoc Dunn's test. Data are expressed as mean±s.e.m. of experiments performed in duplicate using cells from a minimum of three independent donors.

Acknowledgements

We thank the research nurses involved in the study at NNUH for their support.

Competing interests

The authors declare no competing or financial interests.

Author contributions

Conceptualization: J.J.O.T., S.J.F.; Methodology: S.B.A., S.J.F.; Formal analysis: S.B.A., S.J.F.; Investigation: S.B.A.; Data curation: S.B.A.; Writing - original draft: S.J.F.; Writing - review & editing: S.B.A., J.J.O.T., S.J.F.; Supervision: J.J.O.T., S.J.F.; Project administration: J.J.O.T., S.J.F.; Funding acquisition: S.J.F.

Funding

This research is funded by the Biotechnology and Biological Sciences Research Council.

Supplementary information

Supplementary information available online at
http://jcs.biologists.org/lookup/doi/10.1242/jcs.221994.supplemental

References

Ahmadian, M., Wang, Y. and Sul, H. S. (2010). Lipolysis in adipocytes. *Int. J. Biochem. Cell Biol.* **42**, 555-559.

Arruda, A. P. and Hotamisligil, G. S. (2015). Calcium homeostasis and organelle function in the pathogenesis of obesity and diabetes. *Cell Metab.* **22**, 381-397.

Ashour, F. and Deuchars, J. (2004). Electron microscopic localisation of P2X4 receptor subunit immunoreactivity to pre- and post-synaptic neuronal elements and glial processes in the dorsal vagal complex of the rat. *Brain Res.* **1026**, 44-55.

Bartness, T. J., Liu, Y., Shrestha, Y. B. and Ryu, V. (2014). Neural innervation of white adipose tissue and the control of lipolysis. *Front. Neuroendocrinol.* **35**, 473-493.

Bernstein, E. L., Koutkia, P., Ljungquist, K., Breu, J., Canavan, B. and Grinspoon, S. (2004). Acute regulation of adiponectin by free fatty acids. *Metabolism* **53**, 790-793.

Bowers, R. R., Festuccia, W. T. L., Song, C. K., Shi, H., Migliorini, R. H. and Bartness, T. J. (2004). Sympathetic innervation of white adipose tissue and its

regulation of fat cell number. *Am. J. Physiol. Regul. Integr. Comp. Physiol.* **286**, R1167-R1175.
Brand, C. S., Hocker, H. J., Gorfe, A. A., Cavasotto, C. N. and Dessauer, C. W. (2013). Isoform selectivity of adenylyl cyclase inhibitors: characterization of known and novel compounds. *J. Pharmacol. Exp. Ther.* **347**, 265-275.
Cioffi, D. L., Moore, T. M., Schaack, J., Creighton, J. R., Cooper, D. M. F. and Stevens, T. (2002). Dominant regulation of interendothelial cell gap formation by calcium-inhibited type 6 adenylyl cyclase. *J. Cell Biol.* **157**, 1267-1278.
Clapham, D. E. (2007). Calcium signaling. *Cell* **131**, 1047-1058.
Corriden, R. and Insel, P. A. (2010). Basal release of ATP: an autocrine-paracrine mechanism for cell regulation. *Sci. Signal.* **3**, re1.
Gorini, S., Gatta, L., Pontecorvo, L., Vitiello, L. and la Sala, A. (2013). Regulation of innate immunity by extracellular nucleotides. *Am. J. Blood Res.* **3**, 14-28.
Govindan, S. and Taylor, C. W. (2012). P2Y receptor subtypes evoke different Ca2+ signals in cultured aortic smooth muscle cells. *Purinergic Signal.* **8**, 763-777.
Gray, N. E., Lam, L. N., Yang, K., Zhou, A. Y., Koliwad, S. and Wang, J.-C. (2012). Angiopoietin-like 4 (Angptl4) protein is a physiological mediator of intracellular lipolysis in murine adipocytes. *J. Biol. Chem.* **287**, 8444-8456.
Greenberg, A. S. and Obin, M. S. (2006). Obesity and the role of adipose tissue in inflammation and metabolism. *Am. J. Clin. Nutr.* **83**, 461S-465S.
Grynkiewicz, G., Poenie, M. and Tsien, R. Y. (1985). A new generation of Ca2+ indicators with greatly improved fluorescence properties. *J. Biol. Chem.* **260**, 3440-3450.
Halberg, N., Wernstedt, I. and Scherer, P. E. (2008). The adipocyte as an endocrine cell. *Endocrinol. Metab. Clin. N. Am.* **37**, 753-768.
Halls, M. L. and Cooper, D. M. F. (2011). Regulation by Ca2+-signaling pathways of adenylyl cyclases. *Cold Spring Harbor Perspect. Biol.* **3**, a004143.
Heckmann, B. L., Zhang, X., Xie, X., Saarinen, A., Lu, X., Yang, X. and Liu, J. (2014). Defective Adipose lipolysis and altered global energy metabolism in mice with adipose overexpression of the lipolytic inhibitor G 0 /G 1 switch gene 2 (G0S2). *J. Biol. Chem.* **289**, 1905-1916.
Hernandez-Olmos, V., Abdelrahman, A., El-Tayeb, A., Freudendahl, D., Weinhausen, S. and Müller, C. E. (2012). N-substituted phenoxazine and acridone derivatives: structure–activity relationships of potent P2X4 receptor antagonists. *J. Med. Chem.* **55**, 9576-9588.
Hoffmann, K., Baqi, Y., Morena, M. S., Glanzel, M., Muller, C. E. and Von Kugelgen, I. (2009). Interaction of new, very potent non-nucleotide antagonists with arg256 of the human platelet P2Y12 receptor. *J. Pharmacol. Exp. Ther.* **331**, 648-655.
Jacobson, K. A., Ivanov, A. A., De Castro, S., Harden, T. K. and Ko, H. (2009). Development of selective agonists and antagonists of P2Y receptors. *Purinergic Signal.* **5**, 75-89.
Juan, C.-C., Chang, C.-L., Lai, Y.-H. and Ho, L.-T. (2005). Endothelin-1 induces lipolysis in 3T3-L1 adipocytes. *Am. J. Physiol. Endocrinol. Metab.* **288**, E1146-E1152.
Jun, D.-J., Lee, J.-H., Choi, B.-H., Koh, T.-K., Ha, D.-C., Jeong, M.-W. and Kim, K.-T. (2006). Sphingosine-1-phosphate modulates both lipolysis and leptin production in differentiated rat white adipocytes. *Endocrinology* **147**, 5835-5844.
Katada, T., Tamura, M. and Ui, M. (1983). The A protomer of islet-activating protein, pertussis toxin, as an active peptide catalyzing ADP-ribosylation of a membrane protein. *Arch. Biochem. Biophys.* **224**, 290-298.
Kennedy, C. (2015). ATP as a cotransmitter in the autonomic nervous system. *Auton. Neurosci.* **191**, 2-15.
Kim, H. S., Ohno, M., Xu, B., Kim, H. O., Choi, Y., Ji, X. D., Maddileti, S., Marquez, V. E., Harden, T. K. and Jacobson, K. A. (2003). 2-Substitution of adenine nucleotide analogues containing a bicyclo[3.1.0]hexane ring system locked in a northern conformation: enhanced potency as P2Y1 receptor antagonists. *J. Med. Chem.* **46**, 4974-4987.
Kim, Y.-C., Lee, J.-S., Sak, K., Marteau, F., Mamedova, L., Boeynaems, J.-M. and Jacobson, K. A. (2005). Synthesis of pyridoxal phosphate derivatives with antagonist activity at the P2Y13 receptor. *Biochem. Pharmacol.* **70**, 266-274.
Kotnis, S., Bingham, B., Vasilyev, D. V., Miller, S. W., Bai, Y., Yeola, S., Chanda, P. K., Bowlby, M. R., Kaftan, E. J., Samad, T. A. et al. (2010). Genetic and functional analysis of human P2X5 reveals a distinct pattern of exon 10 polymorphism with predominant expression of the nonfunctional receptor isoform. *Mol. Pharmacol.* **77**, 953-960.
Krzyzanowska, K., Mittermayer, F., Krugluger, W., Roden, M., Schernthaner, G. and Wolzt, M. (2007). Adiponectin concentrations increase during acute FFA elevation in humans treated with rosiglitazone. *Horm. Metab. Res.* **39**, 769-772.
La Paglia, L., Listì, A., Caruso, S., Amodeo, V., Passiglia, F., Bazan, V. and Fanale, D. (2017). Potential role of ANGPTL4 in the cross talk between metabolism and cancer through PPAR signaling pathway. *PPAR Res.* **2017**, 1-15.
Lazarowski, E. R., Watt, W. C., Stutts, M. J., Boucher, R. C. and Harden, T. K. (1995). Pharmacological selectivity of the cloned human P2U-purinoceptor: potent activation by diadenosine tetraphosphate. *Br. J. Pharmacol.* **116**, 1619-1627.
Lee, S.-A., Yuen, J. J., Jiang, H., Kahn, B. B. and Blaner, W. S. (2016). Adipocyte-specific overexpression of retinol-binding protein 4 causes hepatic steatosis in mice. *Hepatology* **64**, 1534-1546.
Mamedova, L. K., Joshi, B. V., Gao, Z.-G., Von Kügelgen, I. and Jacobson, K. A. (2004). Diisothiocyanate derivatives as potent, insurmountable antagonists of P2Y6 nucleotide receptors. *Biochem. Pharmacol.* **67**, 1763-1770.
Meis, S., Hamacher, A., Hongwiset, D., Marzian, C., Wiese, M., Eckstein, N., Royer, H.-D., Communi, D., Boeynaems, J.-M., Hausmann, R. et al. (2010). NF546 [4,4'-(Carbonylbis(imino-3,1-phenylene-carbonylimino-3,1-(4-methyl-phenylene)-carbonylimino))-bis(1,3-xylene-, '-diphosphonic acid) tetrasodium salt] is a non-nucleotide P2Y11 agonist and stimulates release of interleukin-8 from human monocyte-deri. *J. Pharmacol. Exp. Ther.* **332**, 238-247.
Micklewright, J. J., Layhadi, J. A. and Fountain, S. J. (2018). P2Y 12 receptor modulation of ADP-evoked intracellular Ca 2+ signalling in THP-1 human monocytic cells. *Br. J. Pharmacol.* **175**, 2483-2491.
Miyoshi, H., Souza, S. C., Zhang, H.-H., Strissel, K. J., Christoffolete, M. A., Kovsan, J., Rudich, A., Kraemer, F. B., Bianco, A. C., Obin, M. S. et al. (2006). Perilipin promotes hormone-sensitive lipase-mediated adipocyte lipolysis via phosphorylation-dependent and -independent mechanisms. *J. Biol. Chem.* **281**, 15837-15844.
Miyoshi, H., Perfield, J. W., Obin, M. S. and Greenberg, A. S. (2008). Adipose triglyceride lipase regulates basal lipolysis and lipid droplet size in adipocytes. *J. Cell. Biochem.* **105**, 1430-1436.
Nelson, D. W., Gregg, R. J., Kort, M. E., Perez-Medrano, A., Voight, E. A., Wang, Y., Grayson, G., Namovic, M. T., Donnelly-Roberts, D. L., Niforatos, W. et al. (2006). Structure–activity relationship studies on a series of novel, substituted 1-benzyl-5-phenyltetrazole P2X 7 antagonists. *J. Med. Chem.* **49**, 3659-3666.
Nielsen, T. S., Jessen, N., Jørgensen, J. O. L., Møller, N. and Lund, S. (2014). Dissecting adipose tissue lipolysis: molecular regulation and implications for metabolic disease. *J. Mol. Endocrinol.* **52**, R199-R222.
North, R. A. (2002). Molecular physiology of P2X receptors. *Physiol. Rev.* **82**, 1013-1067.
Omori, K. and Kotera, J. (2007). Overview of PDEs and their regulation. *Circ. Res.* **100**, 309-327.
Ormond, S. J. (2006). An uncharged region within the N terminus of the P2X6 receptor inhibits its assembly and exit from the endoplasmic reticulum. *Mol. Pharmacol.* **69**, 1692-1700.
Qiao, L., Lee, B., Kinney, B., Yoo, H. and Shao, J. (2011). Energy intake and adiponectin gene expression. *Am. J. Physiol. Endocrinol. Metab.* **300**, E809-E816.
Rafehi, M., Burbiel, J. C., Attah, I. Y., Abdelrahman, A. and Müller, C. E. (2017). Synthesis, characterization, and in vitro evaluation of the selective P2Y2 receptor antagonist AR-C118925. *Purinergic Signal.* **13**, 89-103.
Ronti, T., Lupattelli, G. and Mannarino, E. (2006). The endocrine function of adipose tissue: an update. *Clin. Endocrinol.* **64**, 355-365.
Rosen, E. D. and Spiegelman, B. M. (2006). Adipocytes as regulators of energy balance and glucose homeostasis. *Nature* **444**, 847-853.
Rutkowski, J. M., Stern, J. H. and Scherer, P. E. (2015). The cell biology of fat expansion. *J. Cell Biol.* **208**, 501-512.
Rydén, M. and Arner, P. (2017). Subcutaneous adipocyte lipolysis contributes to circulating lipid levels. *Arterioscler. Thromb. Vasc. Biol.* **37**, 1782-1787.
Shi, H., Halvorsen, Y. I., Ellis, P. N., Wilkison, W. O. and Zemel, M. B. (2000). Role of intracellular calcium in human adipocyte differentiation. *Physiol. Genomics* **3**, 75-82.
Sivaramakrishnan, V., Bidula, S., Campwala, H., Katikaneni, D. and Fountain, S. J. (2012). Constitutive lysosome exocytosis releases ATP and engages P2Y receptors in human monocytes. *J. Cell Sci.* **125**, 4567-4575.
Snyder, P. B., Esselstyn, J. M., Loughney, K., Wolda, S. L. and Florio, V. A. (2005). The role of cyclic nucleotide phosphodiesterases in the regulation of adipocyte lipolysis. *J. Lipid Res.* **46**, 494-503.
Stokes, L. (2013). Rab5 regulates internalisation of P2X4 receptors and potentiation by ivermectin. *Purinergic Signal.* **9**, 113-121.
Sukumar, P., Sedo, A., Li, J., Wilson, L. A., O'regan, D., Lippiat, J. D., Porter, K. E., Kearney, M. T., Ainscough, J. F. X. and Beech, D. J. (2012). Constitutively active TRPC channels of adipocytes confer a mechanism for sensing dietary fatty acids and regulating adiponectin. *Circ. Res.* **111**, 191-200.
Torres, G. E., Egan, T. M. and Voigt, M. M. (1999). Hetero-oligomeric assembly of P2X receptor subunits. *J. Biol. Chem.* **274**, 6653-6659.
Turner, J. J. O., Foxwell, K. M., Kanji, R., Brenner, C., Wood, S., Foxwell, B. M. J. and Feldmann, M. (2010). Investigation of nuclear factor-κB inhibitors and interleukin-10 as regulators of inflammatory signalling in human adipocytes. *Clin. Exp. Immunol.* **162**, 487-493.
Van Harmelen, V., Reynisdottir, S., Cianflone, K., Degerman, E., Hoffstedt, J., Nilsell, K., Sniderman, A. and Arner, P. (1999). Mechanisms involved in the regulation of free fatty acid release from isolated human fat cells by acylation-stimulating protein and insulin. *J. Biol. Chem.* **274**, 18243-18251.
Von Kügelgen, I. and Hoffmann, K. (2016). Pharmacology and structure of P2Y receptors. *Neuropharmacology* **104**, 50-61.

Wang, H., Bell, M., Sreenevasan, U., Hu, H., Liu, J., Dalen, K., Londos, C., Yamaguchi, T., Rizzo, M. A., Coleman, R. et al. (2011). Unique regulation of adipose triglyceride lipase (ATGL) by perilipin 5, a lipid droplet-associated protein. *J. Biol. Chem.* **286**, 15707-15715.

Wedellová, Z., Dietrich, J., Siklová-Vítková, M., Kološtová, K., Kováčiková, M., Dušková, M., Brož, J., Vedral, T., Stich, V. and Polák, J. (2011). Adiponectin inhibits spontaneous and catecholamine-induced lipolysis in human adipocytes of non-obese subjects through AMPK-dependent mechanisms. *Physiol. Res.* **60**, 139-148.

Weisberg, S. P., McCann, D., Desai, M., Rosenbaum, M., Leibel, R. L. and Ferrante, A. W. (2003). Obesity is associated with macrophage accumulation in adipose tissue. *J. Clin. Investig.* **112**, 1796-1808.

Xue, B., Greenberg, A. G., Kraemer, F. B. and Zemel, M. B. (2001). Mechanism of intracellular calcium ([Ca2+]i) inhibition of lipolysis in human adipocytes. *FASEB J.* **15**, 2527-2529.

Yegutkin, G. G. (2008). Nucleotide- and nucleoside-converting ectoenzymes: important modulators of purinergic signalling cascade. *Biochim. Biophys. Acta* **1783**, 673-694.

Zhang, H. H., Halbleib, M., Ahmad, F., Manganiello, V. C. and Greenberg, A. S. (2002). Tumor necrosis factor-alpha stimulates lipolysis in differentiated human adipocytes through activation of extracellular signal-related kinase and elevation of intracellular cAMP. *Diabetes* **51**, 2929-2935.